ADDIS ABABA UNIVERSITY

COLLEGE OF NATURAL SCIENCES

SCHOOL OF EARTH SCIENCES

INTEGRATED GOPHYSICAL INVESTIGATION FOR CHEW BAHIR LAKE BED CHARACTERIZATION, SOUTHERN ETHIOPIA

By

Daniel Mamo Teshome

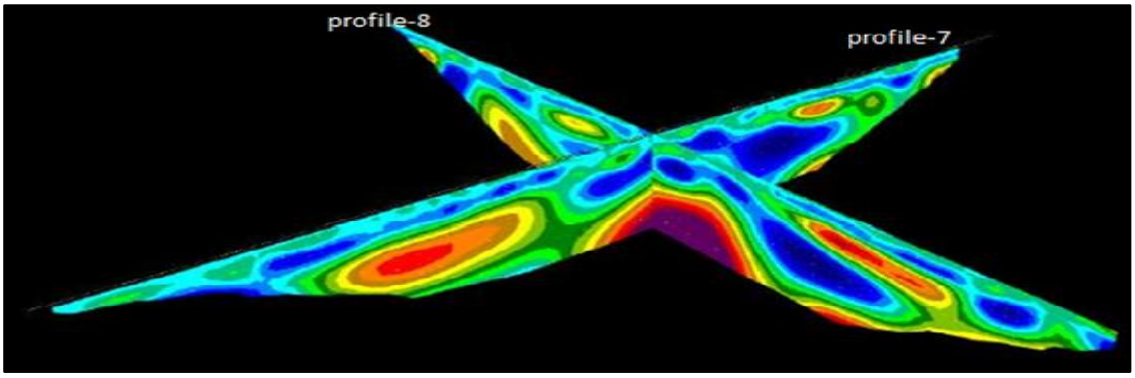

A Thesis Submitted to the School of Graduate Studies of Addis Ababa University in Partial Fulfillment of the Requirements for the Degree of Masters of Science (MSc) in Exploration Geophysics

Addis Ababa

December, 2014

ADDIS ABABA UNIVERSITY

COLLEGE OF NATURAL SCIENCES

SCHOOL OF EARTH SCIENCES

INTEGRATED GOPHYSICAL INVESTIGATION FOR CHEW BAHIR LAKE BED CHARACTERIZATION, SOUTHERN ETHIOPIA

By

Daniel Mamo Teshome

School of Earth Sciences

Approved by Board of Examiners:	Signature	Date
Dr. Abera Alemu Chairman, school of Earth Sciences	_____	_____
Dr. Tigistu Haile Advisor	_____	_____
Dr. Assfawosen Asrat Co-advisor	_____	_____
Dr. Tilahun Mamo Internal Examiner	_____	_____
Dr. Balemual Atnafu External Examiner	_____	_____

December, 2014

Acknowledgments

First of all, I would like to thank the almighty God for the countless blessings.

I have no words to thank my advisor Dr. Tigistu Haile for his pivotal assistance all the way through this thesis work. The productive suggestions he gave me were vital to accomplish the work and this final manuscript. Furthermore, I would like to thank him for organizing financial supports during the fieldwork and, computational facilities like providing different software for processing geophysical data. Your support in suggesting valuable reading materials and in sharing your field and research experiences contributed greatly. Thank you and God bless you.

I would like to express my profound thanks to my co-advisor, Dr. Asfawossen Asrat for his support and comment for the success of this thesis.

I want to acknowledge Dr. Tilahun Mamo and Dr.Abera Alemu for their help in providing some valuable comments and sharing their research experiences.

I extend my acknowledgement to all my friends for their aid in learning the geophysical data processing software and for suggesting other supportive ideas.

Finally yet prominently, my sincere thank goes to my parents who helped me a lot in finalizing this thesis work within the limited time frame.

Abstract

This thesis encompasses ground geophysical investigations and examination of previously collected geophysical data at the Chew Bahir, Chelbi Southern Ethiopia. The objectives of the survey was to characterize the Lake bed and proposed core drill sites and check their suitability for obtaining continuous core samples for paleohistory and paleoenvironmental studies. The earlier collected geophysical data include patented seismic data collected by Tullow Oil Plc. The firsthand field data contain electrical resistivity tomography (ERT) and vertical electrical soundings (VES) data over three locations i.e. at the planned core drill site, at an alternative drill site, and at a location adjacent to the valley sides across one of the major alluvial fans.

Upon analysis, data from the regional seismic show a dipping bedrock surface away from the valley sides towards the basin center with the suggestion of greater than 5km of unconsolidated sediment at the basin center. The electrical imaging field data map the subsurface to an estimated 70 m below the Lake bed. The results revealed very low apparent resistivity within the basin's Lake bed sediments (characteristically less than 1 Ωm), with significantly higher apparent resistivity through the alluvial fan at the valley side (often greater than 500 Ωm). Inside the very low resistivity area, contrary to the expected horizontally stratified subsurface, small lateral resistivity inhomogeneities were exhibited that are possibly associated with lithological changes and changes in desiccation history. The geophysical signature associated with the alluvial fans was clearly distinguished at the valley side, but no signal of similar features was found over the two suggested drill sites. Based on the geophysical survey to date, a location of UTM 261829N and 521120E is recommended for drilling in a sequence of somewhat uniform Lake deposits.

Key words: Electrical Resistivity Tomography, Vertical Electrical Sounding, Seismic Refraction, Inverse Model Sections, Chew Bahir

Table of Contents

List of Figures

List of Tables

List of Appendices

Acronyms

AGC	Automatic Gain Function
CB5	Core Drilling Bore hole five
CMP	Common Mid-Point
DC	Direct Current
DTM	Down the Hole Measurement
ERT	Earth Resistivity Tomography
GPS	Global Positioning System
GRM	General Reciprocal Method
ITCZ	Inter Tropical Convergence Zone
MER	Main Ethiopian Rift
NMO	Normal Move Out
RMS	Root Mean Square
TWT	Two Way Time
UTM	Universal Transverse Mercator
VES	Vertical Electrical Sounding
VNMO	.Normal Move out Velocity
VSP	Vertical Seismic Profile
$\Omega - m$	Ohm-meter

CHAPTER ONE

1. INTRODUCTION

1.1 General

The project area, Chew Bahir is at the southern end of the Ethiopian section of the Great Rift Valley. It lies across the border of South Omo Zone of Southern Nations, Nationalities and Peoples' Region (SNNPS) to the west, and the Borena Zone of Oromiya Region to the East. The Southern tip of the Lake crosses the border into Kenya. The nearest settlement to the Lake, Arbore, is in South Omo Zone, over 130 km South-East of the zonal capital Jinka. The Lake lies in a basin primarily composed of the flood-plains of the Gelana Dulei river, itself formed by the confluence of the Segen and Weyto rivers. Chew Bahir basin and the Gelana Dulei and Weyto valleys are flanked on the West by steep, finely dissected, scarps rising to 1,600 m, the result of large-scale faulting. Lake Chew Bahir is subject to substantial changes in area as a result of variations in river discharge. It often dries out, but the lowest part in the North-East is always moist. As there is no outlet, all water entering the Lake is lost by evaporation. Over the past century, Chew Bahir has varied from swamp to shallow open water with a maximum depth of 7.5 m and a surface area of up to 2,000 km² (http://www.birdlife.org).

The water of Chew Bahir is so highly saline that it cannot be used for either irrigation or domestic purposes. However, to the south-east across the mudflats lie a series of springs: some occur around the base of rock outcrops, but others are isolated on the flats where they support a dense growth of course, salt-tolerant sedge. The Arbore, Tsemay and Hamer peoples inhabit the Weyto valley and Chew Bahir basin. They are basically pastoralists, but grow some crops opportunistically. Access to the freshwater springs in and beside the Lake is disputed (Birchall et al., 1975).

The main essence of this project is to map the upper most Lake bed and characterize the upper most layers using integrated geophysical methods like electrical (Electrical Resistivity Tomography, ERT and Vertical Electrical Sounding, VES) and seismic methods and identifying geophysical signature of the Lake bed more appropriately So that the scientific communities can gain a lot from the study.

1.2 Description of the study area

1.2.1 Location

The study area is located at the end of the Ethiopian section of the Great Rift Valley. It lies across the border of South Omo Zone of Southern Nation, Nationalities and Peoples' Region to the West, and the Borena Zone of Oromiya region to the East, as shown in figure. It is bounded by Geographical UTM coordinates of approximately between 4.1-6.3^{0}N latitude and 36.5-38.1^0 E longitude.

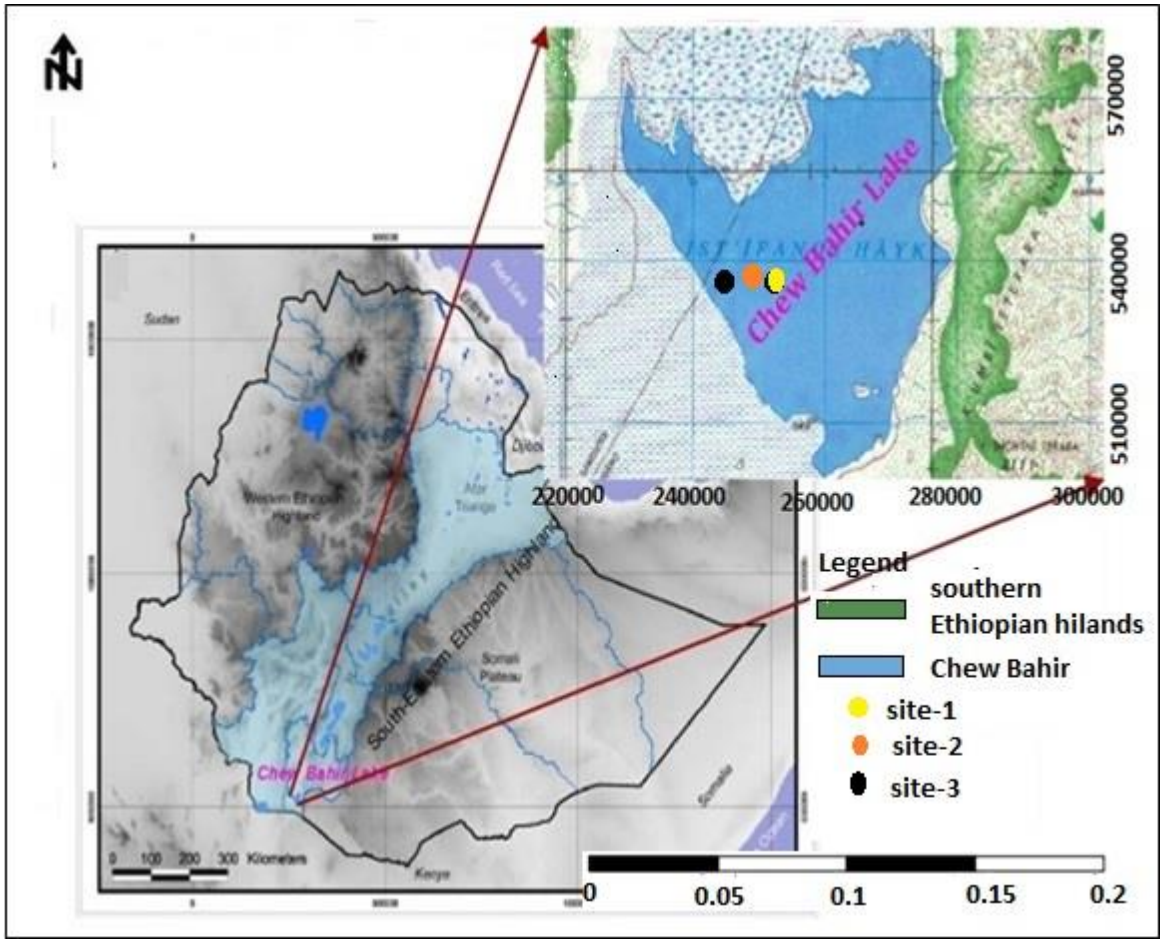

Figure 1. 1 Location map of Chew Bahir, South Ethiopia.

1.2.2 Topography

The area lies in a 300 km wide rift zone, between the Omo-Turkana basin to the West and the Southern sector of the main Ethiopian Rift (MER) to the East. The MER splits into two branches south of the Lake Abaya-Chamo basin, separated by the Amaro horst. The Eastern branch forms the Southernmost sector of MER. In the Western sector, rift faulting dies out at the Southern shore of Lake Chamo close to the Konso uplands, but

resumes farther West in the Chew Bahir basin. The Chew Bahir basin extends south to the Kenyan Rift and forms the northernmost part of the broadly rifted zone that was formed when rifting migrated eastward along pre-rift structures of the Anza rift (Ebingeer et al., 2000; Corti, 2009).

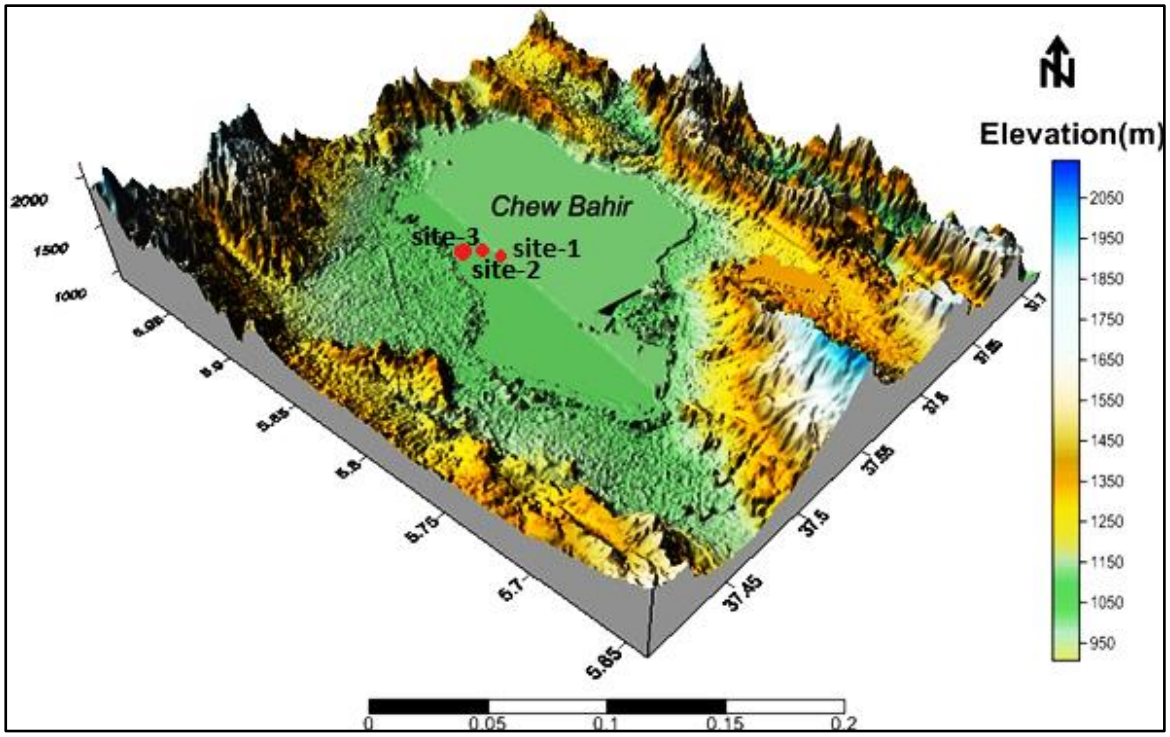

Figure 1. 2 Topographic map of the study area, Chew Bahir, South Ethiopia.

1.2.3 Climate

The climate of East Africa is characterized by strong rainfall seasonality, which results from the annual migration of the intertropical convergence Zone (ITCZ) between 10° North and South, following the zenithal position of the sun (Nicholson,1996). Because of this migration, bimodal rains dominate the northeast the "Belg" rains from March to May, and the longer "Kiremet" rains from June to September .In the highlands northwest of Chew Bahir, rainfall is uni-modal with one wet season from March to November (Segele and Lamb, 2005; Williams and Funk, 2011). Chew Bahir lies in a transition zone between the influences of tropical equatorial and summer monsoonal climates, and between two major systems that bring precipitation from the Indian and Atlantic oceans (Forster et al.,2012).

1.3 Problem statement

Rainfall and the runoff produce washes soil into rivers, which flow into Lakes. As the moving river water, with its suspended sediments, reaches the calmer Lake or ocean environment, the sediments fall to the bottom, gradually building up layer upon layer of deposits. Likewise, fine grains from distant dust storms and ash from far-off volcanoes can be blown over water, fall to the surface, and sink to the bottom to join the deposition process. Organic materials from creatures living within the water column also rain down upon the depths to join the muck at the bottom, particularly in deep-ocean environments.

Some types of deposition processes have seasonal cycles that leave annual layers in the sediments similar to tree ring patterns or ice core layers. For instance, sediments in rivers tend to arrive in greater quantities and to be of a different color during spring runoff than during the rest of the year when flow rates are lower. Sediment deposits strongly influenced by input from rivers thus can display annual layers (Frank et al., 1999).

The project area, Chew Bahir, is a dry Lake at the end of the Ethiopian section of the Great Rift Valley which forms its layers mainly by washes of soil of rainfall, runoff and Eolian input mainly of silt.

Figure 1. 3 Partial view of the site, Chew Bahir lake bed.

Studying each layer provides some data sets for the ongoing project around the area and different scientific communities at large. Before starting any geo-scientific investigation on the area it needs acquiring information about the geology, geological structures and hydrogeology of the site but due to inhomogeneity of the material below the Earth's surface, the extrapolation/interpolation of the results obtained from the limited number of test drill holes is not representative results over a larger area.

Geophysical methods help to resolve the above problems and are capable of producing better extrapolations of whole area below the surface of the Earth by taken denser spacing measurements than direct sampling. These conditions motivate to conduct integrated geophysical methods for better understanding of the subsurface properties of Earth layers in the study area, Chew Bahir.

1.4 Objectives of the Study

1.4.1 General Objective

The main objective of this research is to conduct detailed geophysical investigations to image the subsurface geology and to characterize the different succession of the Chew Bahir Lake bed and also for mapping and identifying linear geologic features in terms of their geophysical signatures.

1.4.2 Specific Objectives

The specific objectives of this project are:

- To characterize the upper most succession of Chew Bahir Lake bed,
- To map the presence, lateral and vertical extent of geological features,
- To suggest the appropriate location for drilling of a borehole to be used for the ongoing study (paleoenvironmental reconstruction team) around the area, and
- To know the extent as to how far the electrical methods of prospecting are viable for the highly conducting top surface Lake bed characterization.

1.5 Significance of the study

The main significance of this project is to map the dry Lake bed and characterize each layer using integrated geophysical methods like electrical and seismic methods and in addition it indicates weather the method of geophysics we use is more appropriately mapping Lake beds like Chew Bahir so that it can help the drilling team of the ongoing

project around the area (paleoenvironment reconstruction) regarding the indication of conformable sedimentation for better core sampling and having geophysical data sets for scientific community around the area at large .

1.6 Methodology

The methodology followed in the existing research processes is based on the objective formulated in section 1.4. Geophysical methods of investigation were employed in which, the electrical resistivity: Electrical tomography, vertical electrical sounding and seismic techniques used. The 2D electrical resistivity imaging and vertical electrical data were collected along the profiles. The spatial geophysical mapping and modeling has been assisted using software's such as, RES2DINV, PROSYS-II, ArcGIS-10, Global Mapper Strater, Map Info, AutoCAD and Surfer10 software mainly applied for map interpretation and modeling. The generalized flow chart of methodological approach is described in figure 1.4.

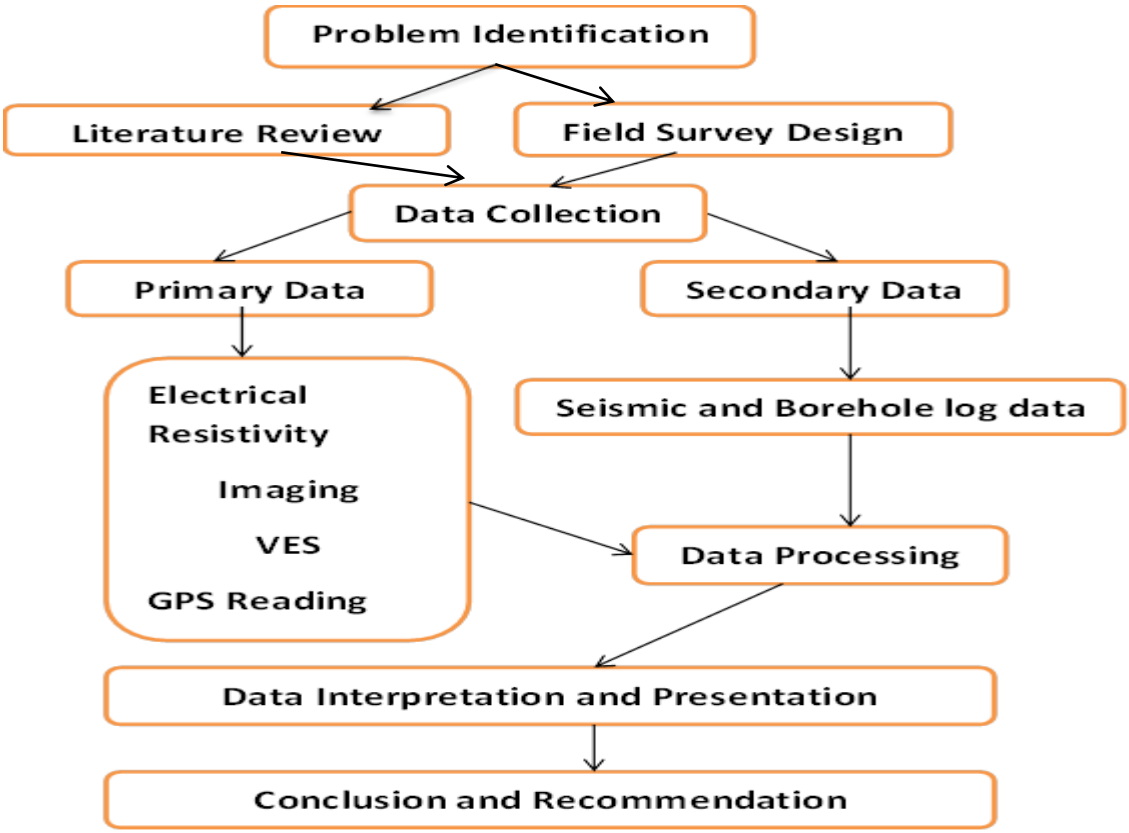

Figure1. 4 Flow chart showing the general methodological approach used for the thesis work.

1.7 Previous Works

In the past few years geological, hydrogeological and geophysical studies and other related works have been performed for different purposes in the study area and its surrounding. The purpose of those studies was mostly concerned with mineral and hydrocarbon exploration, and paleo environment reconstruction .A number of works has been done by different scholars. Some of the relevant works are:

1. The Chew Bahir Drilling Project: A Plio-Pleistocene Climate record from the Southern Ethiopian Rift, a Crucible of Human Evolution. Proposal for the ICDP-HSPDP (Hominin Sites and PalaeoLakes Drilling Project), pp. 1-8 (Asfawossen Asrat et al., 2009)
2. Omo River Project, a joint Ethiopia-Canada geological and geochemical reconnaissance survey in southwest Ethiopia (Davidson, 1983).
3. Paleomagnetism of Lake sediments, Chew Bahir, Ethiopia conducted by Frank et al., (2011).
4. Provenance Analysis of Surface Sediments in the Chew Bahir Basin (Ethiopia) using Remote Sensing Data conducted by Boesche and Trauth (2012).
5. Climatic change recorded in the sediments of the Chew Bahir basin, southern Ethiopia, during the last 45,000 years conducted by Foerster et al., (2012).
6. Well-testing in the Shimela exploration well being drilled near Chew Bahir, conducted by Tullow Oil plc. (2011).

1.8 Arrangement of the thesis

This thesis is organized in to six chapters. The first chapter is general introduction of the study, its objective and the methodological approach. The second chapter is concerned mostly with the work of previous researchers that includes geology, of the study area and its surrounding. Chapter three covers the theoretical background for the geophysical methods employed in this study. Chapter four describes the complete survey procedure, data acquisition, data processing, and presentation of the different results. Chapter five covers integrated results, discussion and interpretations of geophysical methods. The last chapter contains conclusions and recommendations of the research work.

CHAPTER TWO

2. GEOLOGY OF THE STUDY AREA

2.1 Geological overview

The Chew Bahir basin lies in a 300 km extensive rift zone, among the Omo-Turkana basin to the West and the southern segment of the Main Ethiopian Rift (MER) to the East (Figure 2.1). The MER splits into two branches south of the Lake Abaya Chamo basin, parted by the Amaro horst. The eastern branch forms the southernmost division of the MER. In the western sector, rift faulting dies at the southern shore of Lake Chamo nearby to the Konso uplands, but continues farther West in the Chew Bahir basin. The Chew Bahir basin spreads south to the Kenyan Rift and forms the northernmost part of the broadly rifted zone that was formed when rifting migrated eastward along pre-rift structures of the Anza Rift (Ebinger et al., 2000).

The western margin of Chew Bahir basin, the Hammar range, comprises of Precambrian basement with principally undivided gneisses (units "Pebh" and "Pegh" in Figure 2.1). This comprises feldspare-biotitee-muscovite and hornblende gneisses dominating the Hammar range geology, migmatitic in part, with slight metasedimentary gneiss (Pegb), quartzo-feldspathic gneiss, amphibolites and granitoid orthogneiss, layered biotite-quartze-feldspar gneiss, locally with muscovite, garnet, sillimanite, minor interlayered amphibolithic quartzose inclusions (Davidson, 1983). In addition, Precambrian layered mafic gneiss (Pegh) and amphibolite or comparable granulite facies (Pgh) occur in the Hammar range as well as north of the basin. The upper eastern boundary of the Chew Bahir basin, the escarpment of the Teltele-Konso range, depicts Miocene basalts and trachytic centers (unit "NM" in Figure 2.1). Miocene basaltic lava courses with subordinate rhyolite trachyte and felsic tuff intercalations prevail in the eastern part of the catchment. Oligocene basalt flows with minor rhyolites, trachytes, tuffs and ignimbrites (unit "Pv" in Figure 2.1) cover the Precambrian basement units in the northeastern, northern and northwestern parts of the catchment (Figures 2.1; Moore and Davidson, 1978; Davidson, 1983). The tectonically-formed basin provides a sedimentary documentation that extends beyond the Quaternary as the basin begun during older phases of rifting. The total sediment infill of the basin is about 5 km thick, according to airborne

gravity and seismic reflection data (Asfawossen Asrat et al., 2009). A detailed spatial and temporal quantification of uplift and denudation along the Hammar and Teltele ranges adjoining the Chew Bahir basin showed that rifting has been continuous since its beginning in the Miocene, while PlioPleistocene rifting and uplift was not important in this part of the East African Rift (Ebinger et al., 2000; Pik et al., 2008). It was further recommended that direct evidence of denudation is inconsistent with the hypothesis that massive Plio-Pleistocene rifting and associated uplift occurred in this part of the East African Rift and could have triggered recent aridification. Other studies (e.g., Ebinger et al., 2000) also suggested similar ages and processes of rifting for this basin. In short, recent tectonic uplift had little influence on the short-term climatic variations.

Currently, Chew Bahir is a 30 km by 70 km saline mudflat that periodically fills to a shallow Lake during the wet period, with water and sediment contribution by the perennial Weyto and Segen rivers, which have about 2000 Km^2 catchment. Their influence is nowadays limited to the northern part of the basin, where the rivers have formed a delta. Secondary, contributions to the sediment inflow are alluvial fans draining from the Hammar Range to the West and the Teltele Plateau to the East. Small drainage complexes at the border faults, and the strong precipitation seasonality, make sediment and water influx highly periodic, because runoff is largely from extreme rainfall events in the wet seasons, and from irregular orographic rainstorms. Eolian input, mainly of silt, may be significant, particularly through dry times, and can be considered as a fourth sediment source. Eolian activity may also cause erosion and thus pauses in the sedimentary record. Winds carrying material from nearby regions, and redeposit silts within the Chew Bahir basin itself. Minor sources of sediment are volcanic materials, deposited either as pyroclastic air fall deposits, or as reworked tephra. No volcanic centers are bare within the Chew Bahir basin. Tephrochronological correspondences between the Indian Ocean, the Middle Awash and the Omo-Turkana basin signify explosive volcanic events that affected the whole region.

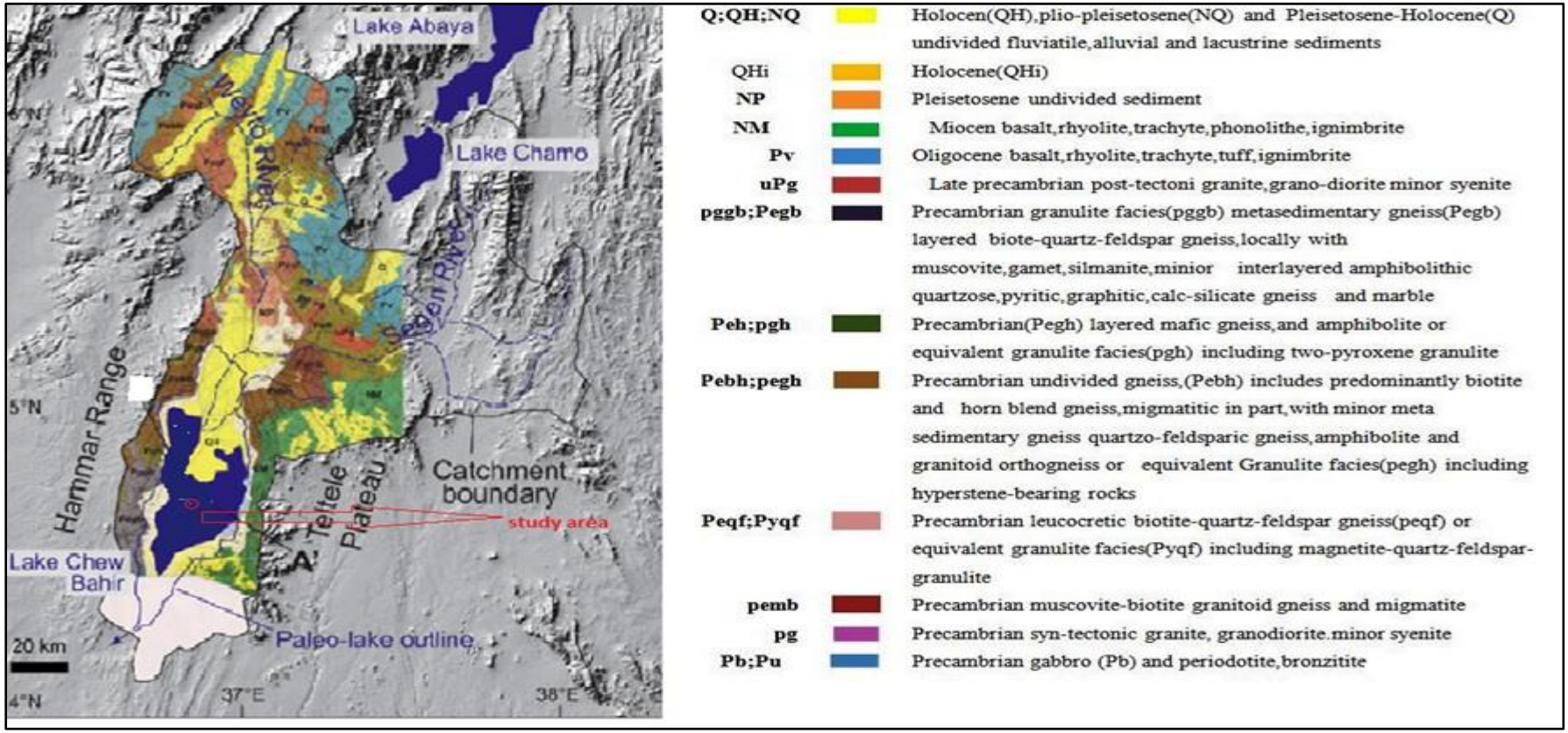

Figure 2. 1 Geological map of the Chew Bahir basin (after Davidson, 1983).

CHAPTER THREE

3. THEORETICAL BACKGROUND OF THE METHODS OF INVESTIGATION

3.1 Direct Current Resistivity Method

3.1.1 Introduction

Electrical resistivity methods were established in the early 1900s but have come to be very much more widely used since the 1970s, due to the diverse use of computers to process and analyze the data using different algorithms. These techniques are used extensively in the search for suitable groundwater sources; in engineering survey to locate subsurface cavities, faults and fissures; in archaeology for mapping the areal extent of remnants of buried foundation of the ancient buildings, amongst many applications (Reynolds, 1997). The purpose of electrical surveys is to determine the subsurface resistivity distribution by taking measurements on the ground surface. From these measurements, the true resistivity can be estimated. The ground resistivity is related to various geological parameters such as the mineral and fluid content, porosity, nature and degree of water saturation in the rock (Loke, 1999).

3.1.2 Fundamental Principle of DC Resistivity

Electrical resistivity survey is based on the principle that the distribution of electrical potential in the ground around a current-carrying electrode, depends on the electrical resistivity and distribution of the surrounding soils and rocks. The usual practice in the field is to apply an electrical direct current (DC) between the two current electrodes deployed in the ground and to measure the potential difference between the two potential electrodes. If we consider a continuous flow of current in voluminous media, the flow of current in the medium is based on the principles of conservation of energy (Kunetz, 1996)

$$(I_C)_S = -\frac{dQ}{dt} \tag{3.1}$$

where Ic is the current flowing out of the closed surface ‘S’ and ‘Q’ is the charge enclosed by ‘S’ The current Ic and Q can be expressed in terms of the current density (J) and the charge density (q) as follows.

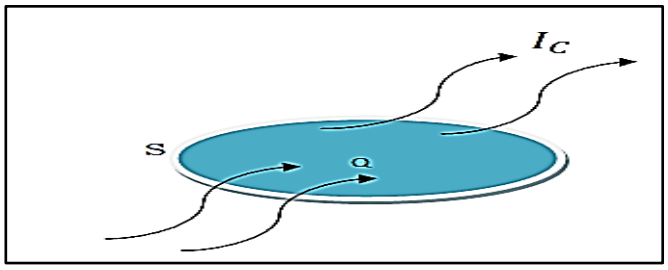

Figure 3. 1 Current flowing out of the closed surface.

$$I_c = \oint J.ds$$

and

$$Q = \int q.dv \tag{3.2}$$

where *v* is the volume bounded by the surface's'. Substituting the equation (3.2) in to the equation (3.1), equation (3.1) becomes

$$\int J.ds = \frac{d}{dt}\int q.dv \tag{3.3}$$

Applying the divergence theorem on the left hand side of the above equation, and interchanging the differentiation and integration sequence on the left hand side of the equation

$$\oint J.ds = (\nabla.J)dv \tag{3.4}$$

$$\int_v^1 (\nabla.J)dv = \int (\frac{\partial q}{\partial t})dv \Leftrightarrow \int (\nabla.J + \frac{\partial q}{\partial t})dv = 0 \tag{3.5}$$

Since equation (3.5) valid for any volume, it can be written as

$$\nabla.J + \frac{\partial q}{\partial t} = 0 \tag{3.6}$$

Equation (3.6) is the law of conservation of charge in differential form, also known as the continuity equation. For stationary value (i.e. direct current), $\frac{\partial q}{\partial t} = o$ and electric field (*E)* is conservative. The electric field can be expressed as the gradient of scalar potential $E = (-\nabla.V)$.The Ohm's law can be written in terms of electric field strength (E***)*** and current density (***J)*** as, $J = -\sigma E$,where ***E*** is measured in volts/meter and σ is conductivity. Conductivity is the reciprocal of resistivity (ρ). For isotropic media, ρ is a scalar function of the point of observation and ***J*** is in the same direction as ***E***. Equation (3.6) is reduces to

$$div\left(\frac{1}{\rho} grad.v\right) = grad\,\frac{1}{\rho}.gradV + \frac{1}{\rho} div.gradV = 0 \qquad (3.7)$$

This equation is called fundamental equation of electrical prospecting with direct current. For homogenous medium, ρ is independent of the coordinate axes and equation (3.7) is simplified as

$$\nabla^2.V = 0 \qquad (3.8)$$

This is called Laplace equation. Therefore, the electrical potential distribution for direct current flow in a homogeneous isotopic medium satisfies the Laplace equation. The Laplace equation has different forms in different coordinate systems as illustrated below.

Cartesian (orthogonal) coordinate system

$$\frac{\partial^2 V}{\partial x^2} + \frac{\partial}{\partial}\frac{^2V}{y^2} + -\frac{\partial^2 V}{\partial Z^2} = 0 \qquad (3.9)$$

Cylindrical coordinate system

$$\frac{\partial^2 V}{\partial r^2} + \frac{1}{r}\frac{\partial V}{\partial r} + \frac{1}{r^2}\frac{\partial^2 V}{\partial \theta^2} = 0 \qquad (3.10)$$

Spherical coordinate system

$$\frac{1}{r^2}\frac{\partial}{\partial r}\left(\frac{\partial V}{\partial r}\right) + \frac{1}{r^2 \sin\theta}\frac{\partial}{\partial \theta}\left(\sin\theta \frac{\partial V}{\partial \theta}\right) + \frac{1}{r^2 \sin^2\theta}\frac{\partial^2 V}{\partial \phi^2} = 0 \qquad (3.11)$$

For hemispherical current distribution, the potential due to single electrode is a function of r only, where r is the distance from the current source to any equipotential surface. Under these conditions the Laplace equation in the spherical coordinates is our concern. Since, the potential is only as function of r; consequently, $\frac{\partial V}{\partial \theta}$ and $\frac{\partial V}{\partial \phi}$ are zero, then equation (3.11) is reduced to:

$$\nabla^2 V = \frac{d^2V}{dr^2} + \frac{2dV}{rdr} \tag{3.12}$$

Multiplying the equation (3.12) by r^2, then integrating twice both sides of this equation gives

$$V = -\frac{A_0}{r^2} + A_1 \tag{3.13}$$

Where, A_0 and A_1 are integration constants and can be solved by using the boundary conditions as follows.

1. Since V= 0 as $r \to \infty$, then A_1=0

2. $\frac{dV}{dZ} = 0$ at Z = 0

3. The current flows radially outwards in all directions from the point electrode. Thus, the total current crossing a hemispherical surface of radius 'r' is given by $I = 2\prod r^2 J$.

$J = \delta E = -\frac{1}{\rho}\frac{dV}{dr}$ and $\frac{dV}{dr} = \frac{A_0}{r^2}$, so. $J = -\frac{1}{\rho}\frac{dV}{dr}$ Substituting these equations in to the equation (3.11) and reduced to

$$\frac{I\rho}{2\prod}\left(\frac{1}{r}\right) \tag{3.14}$$

In practice there are always two current electrodes- a positive one through which the current enters to the ground and a negative one to which it returns. Further, we measure potential difference, that is, a voltage difference. In a homogeneous earth, the current flows radially outward from the source to define a hemispherical surface. The current

distribution is equal everywhere on this surface which is also called an equipotential surface. Figure 3.2 shows the arrangement of current and potential electrodes, current lines and equipotential surfaces in a homogenous isotropic ground when the direct current source is used.

The goal of resistivity survey is to measure the potential difference between two potential electrodes due to the current from two current electrodes. The potential at each electrode is determined due to the current sources. Suppose that the two current and the two potential electrodes *C1*, *C2*, and *P1*, *P2* respectively are in one line as in Figure 3.2b. *C1* being the positive, *C2* the negative current electrode and *k* is the geometric factor, then the potential difference is:

$$\nabla V = V_1 - V_2 = \frac{I\rho}{2\prod}\left(\frac{1}{r_1} - \frac{1}{r_2} - \frac{1}{r_3} + \frac{1}{r_4}\right)$$

$$\nabla V = k\frac{I\rho}{2\prod} \tag{3.15}$$

3.1.3 Correspondence of geology and resistivity

Resistivity survey gives a representation of geo-electric dissemination of the sub surface. To translate the geo-electric layers into a geological cross-sections, information of typical resistivity values for different kinds of subsurface materials and the geology of the area surveyed, is significant. The resistivity of the geological materials exhibits one of the largest ranges of all physical properties, from $1.6\,x\,10^{-8}\Omega m$ for natural silver to $10^{6}\Omega m$ for uncontaminated sulphur. Igneous and metamorphic rocks naturally have high resistivity values (Loke, 1997).

The resistivity of these rocks is greatly dependent on the degree of fracturing, and the percentage of the fractures filled with ground water. Sedimentary rocks, which usually are more porous and have higher water content, normally have lower resistivity values. There are overlap of resistivity values of the different classes of rocks and soils. This is because the resistivity of a particular rock or soil sample depends on a number of factors such as the porosity, the degree of water saturation and the concentration of dissolved salts. The resistivity values of common rocks and soil materials (Loke, 2004) are presented in Appendix.

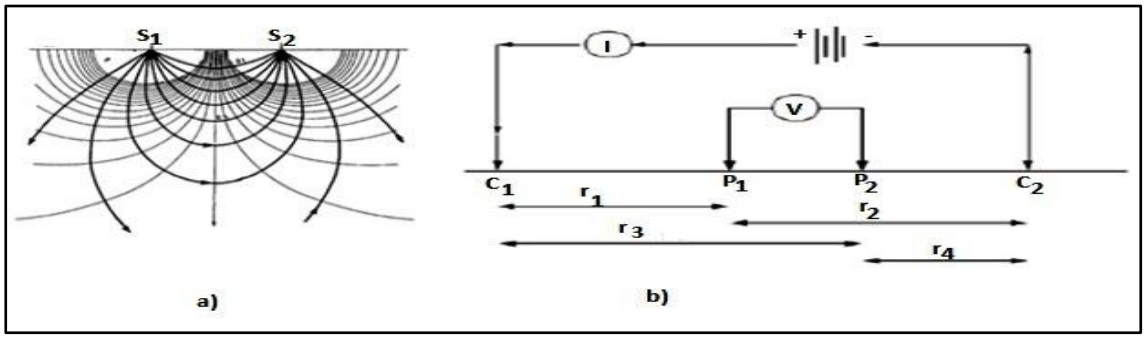

Figure 3. 2 a) Current and equipotential lines produced by a current source and sink, b) Generalized form of electrode configuration in resistivity surveys to measure the subsurface resistivity (after Loke, 1997)

3.1.4 Resistivity Sounding Principle

In resistivity sounding, which is also known as Vertical Electrical Sounding (VES), the positions of electrodes changed with respect to a fixed point (known as the sounding point) and the measured values reflect the vertical distribution of resistivity values on a geologic section.

Vertical electrical sounding (VES) consists of a symmetrical electrode array used to determine the resistivity of the subsurface which is assumed to be horizontally stratified layers. The procedure is used to determine the variations in resistivity in the vertical direction and called electrical drilling or commonly vertical electrical sounding (VES). By expanding symmetrically the distance between current electrodes about a point called the sounding point, while keeping the potential electrodes MN at the same position, provides a sounding curve corresponding to the apparent resistivity versus depth of the location. As the spacing between the current electrode increases, the investigated depth will also increase. The two most commonly used arrays in electrical sounding survey are the Wenner and Schlumberger arrays. In this thesis, we have used the data which was collected by using the Schlumberger electrode array techniques for vertical electrical sounding and both wenner and schlumberger for electrical resistivity tomography (ERT). During Schlumberger electrode arrangement, the distance between the potential electrodes is not greater than one tenth of the current electrodes spacing. The advantage of this array is that initially only the spacing between the current electrodes is increased.

However, at large current electrode spacing, the measured potential becomes very low and the distance between the potential electrodes is increased. Increasing the potential electrode spacing produces 'step' in the apparent resistivity curve and it is good practice to obtain an overlap between the curve segments by obtaining two readings at different potential electrode spacing for two adjacent current electrode spacing. Segments obtained at larger potential electrode spacing can be shifted in order to produce a smooth curve (Gibson and George, 2003).

In electrical prospecting the problem is determining the depth and the electrical resistivity of a series of horizontal or nearly horizontal ground. In order to solve this problem, we should calculate the potential and the electric field, due to a point source of current, at any point on the surface of a stratified earth. This has advantages because of enables one to use axial symmetry of the potential filed about the vertical axis through the current source and the additiveness of the potential is also be used.

Let as choose a cylindrical system of coordinate with the origin at the point source a direct current located on the surface. The subsurface consists of infinite number of layers separated by horizontal boundary planes; the deepest layer existing to infinite depth ($h_n \to \infty$) and the other layers have finite thickness $h_i = h_1, h_2, h_3, \ldots h_n$ and resistivity $\rho_1, \rho_2, \rho_3, \ldots \rho_n$. Each of the layers is electrically homogeneous and isotropic.

The derivative of the potential based on the above conditions was first due to Stefanescu et al., (1930).

$$\frac{\partial^2 V}{\partial x^2} + \frac{\partial^2 V}{\partial y^2} + \frac{\partial^2 V}{\partial z^2} = 0 \qquad (3.16)$$

The potential field has a cylindrical symmetry with respect to the vertical axis line through the current source therefore, Laplace equation in cylindrical coordinate is most appropriate.

For a solution symmetrical with respect to the vertical axis

$$\frac{\partial V}{\partial \theta} = \frac{\partial^2 V}{\partial \theta^2} = 0 \text{ So,}$$

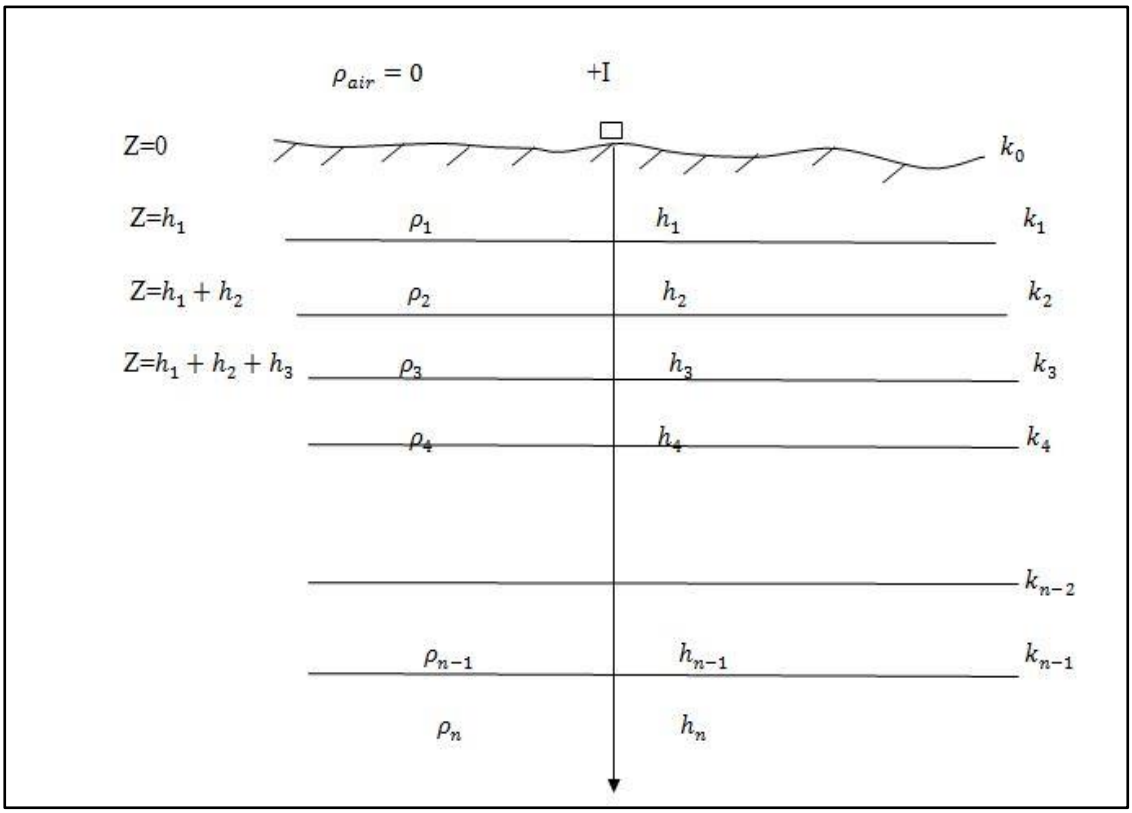

Figure 3. 3 A multi-layer Earth and problem presentation for solution of the potential.

The electrical potential field V for direct current satisfies the differential equation of Laplace, Which is

$$\frac{\partial^2 V}{\partial r^2} + \frac{1}{r}\frac{\partial V}{\partial r} + \frac{\partial^2 V}{\partial z^2} = 0 \tag{3.17}$$

The particular solution of equation (3.18) can be obtained using the method of separation of variables and can be assumed to be of the form:

$$V(r,z) = U(r)W(z) \tag{3.18}$$

Substituting equation (3.18) to (3.17) and dividing throughout by the product U(r) W (z) gives

$$\frac{1}{u(r)}\frac{d^2u(r)}{dr^2} + \frac{1}{ru(r)}\frac{du(r)}{dr} + \frac{1}{w(z)}\frac{d^2w(z)}{dz^2} = 0 \tag{3.19}$$

This equation is satisfied if and only if

$$\frac{1}{u(r)}\frac{d^2u(r)}{dr^2}+\frac{1}{ru(r)}\frac{du(r)}{dr}=\lambda^2, \tag{3.20}$$

and

$$\frac{1}{w(z)}\frac{d^2w(z)}{dz}=-\lambda^2 \tag{3.21}$$

where **λ** is an arbitrary constant

The solution of equation (3.21) may be given as

$$w(z)=c_1e^{+\lambda z} \text{ and } w(z)=c_1e^{-\lambda z} \tag{3.22}$$

and that of equation (3.21) is given

$$U(r)=c_3J_0(\lambda r) \tag{3.23}$$

Where Jo is the Bessel function of order zero

The combination of equation (22) and (23) gives the particular solution of the deferential equation given by equation (3.17), which is

$$V(r,z)=c_5e^{+\lambda z}J_0(\lambda r)$$

$$V(r,z)=c_6e^{-\lambda z}J_0(\lambda r) \tag{3.24}$$

where c and λ are both constants in the last of these equations

Since, by theory of differential equation, every linear combination of the particular solution is also a solution, one can make λ to rough all possible values from 0 to ∞ and allowing the constant "c" to very independence of λ the general solution of equation (3.18) can be obtained as

$$V(r,z)=\int_0^\infty\left[\phi(\lambda)e^{-\lambda z}+\psi(\lambda)e^{-\lambda z}\right]J_0\lambda(r)d\lambda \tag{3.25}$$

Here ϕ(λ)and ψ(λ) are arbitrary functions of .the boundary conditions control the special form of these equations .

From the basic theory, the potential generated by a single point source of current intensity "I" located at the surface of an electrically homogeneous earth is given by

$$V = \frac{I\rho}{2\prod}\frac{1}{\sqrt{r^2+z^2}} \tag{3.26}$$

where ρ is the resistivity of homogeneous Earth.

Equation (3.26) can be written in integral form by using the so-called Lipschitz integral (also called the Weber Integral Formula) in theory of Bessel function as

$$\int_0^\infty e^{-\lambda z} J_0(\lambda r) d\lambda = \frac{1}{\sqrt{r^2+z^2}} \tag{3.27}$$

So that the equation (3.27) gives

$$V = \frac{I\rho}{2\prod}\int_0^\infty e^{-\lambda z} J_0(\lambda r) d\lambda \tag{3.28}$$

Equation (3.27) is also a solution of equation (3.28). Therefore, the combined solution will also be a solution to the equation, that is

$$V(r,z) = \frac{I\rho}{2\prod}\int_0^\infty \left[e^{-\lambda z} + \theta(\lambda)e^{+\lambda z}\right] J_0(\lambda r) d\lambda \tag{3.29}$$

Where Θ(λ) and x(λ) are arbitrary function of λ. Solutions of equation (3.29) are valid in all the layers of the subsurface however, necessarily the same in the different layers of the subsurface. Therefore, the potential due to a point source of current at the surface of a horizontally layered earth must in each layer satisfy

$$V_i(r,z) = \frac{I\rho}{2\prod}\int_0^\infty \left[e^{-\lambda z} + \theta_i(\lambda)e^{+\lambda z} x_i(\lambda)e^{+\lambda z}\right] J_0(\lambda r) d\lambda \tag{3.30}$$

This equation is called the Stefanescu Integral, with I referring to the several layers of the subsurface.

Boundary conditions

For a potential set up by a single source of current at the surface of a horizontally stratified earth

1. At each of the boundary planes in the subsurface, the electrical potential must be the same $V_i = V_{...}$ at $Z = h_i$ (3.31)

2. The vertical component of the current density must be continuous on each boundary plane (the current density normal to the boundary planes …)

$$\left(J_i\right)_N = \left(J_{i+1}\right)$$

$$\frac{1}{\rho_i}\frac{\partial V_i}{\partial x} = \frac{1}{\rho_{i+1}}\left(\partial V_{i+1}\right)/\partial z \qquad (3.32)$$

3. At the surface (z=0) the vertical component of the current density J_v (and hence that of the electric field intensity) must be zero everywhere except in the infinitesimal neighborhood around the current source. (In air J_{air}= 0 and from condition (2), the vertical component of the current density at depth zero must be zero) near the current source the potential must not approach infinity (must remain finite) as

$$V = \frac{I\rho}{2\prod}\frac{1}{\sqrt{r^2 + z^2}} \text{ at depth 0, Z =0, as } r \to 0$$

4. At infinite depth, the potential must approach zero, i.e. V →0 as Z→ ∞

3.1.4 2-D electrical imaging survey

3.1.4.1 Introduction

In recent times, a new idea of instrumentation and data acquisition has been familiarized to make it possible the acquisition of many readings in a reduced amount of time specifically for environmental applications corresponding to shallow studies, depths of the order of 10 to 80m. The method is sometimes called Electrical Resistivity

Tomography (ERT). The concept involves using multi-core cables which contain as many individual wires as number of electrodes, with one take-out every 5m, 10m … and 24, 48, 72, 96 … electrodes.

The measuring unit includes relays which automatically carry out the sequences of readings introduced in its internal memory. The aim of this set-up is to take readings for many combinations of transmission and reception pairs, so as to achieve some kind of mixed wenner / schlumberger array. In such a way of proceeding, the total length of cable is the product of the electrode spacing by the number of electrodes. The greatest limitation of the resistivity sounding method is that it does not take into account horizontal changes in the subsurface resistivity. A more accurate model of the subsurface is a two-dimensional (2-D) model where the resistivity changes in the vertical direction, as well as in the horizontal direction along the survey line. In this case, it is assumed that resistivity does not change in the direction that is perpendicular to the survey line. In theory, a 3-D resistivity survey and interpretation model should be even more accurate. However, at the present time, 2-D surveys are the most practical economic compromise between obtaining very accurate results and keeping the survey costs down (Loke, 1999).

3.1.4.2 Instrumentation and field surveys

One of the new developments in recent years is the use of 2-D electrical imaging/tomography surveys to map areas with moderately complex geology (Griffiths and Barker, 1993). Such surveys are usually carried out using a large number of electrodes, 25 or more, connected to a multi-core cable. At present, field techniques and equipment to carry out 2-D resistivity surveys are well developed.

Figure 3.4 shows the typical setup for a 2-D survey with a number of electrodes along a straight line attached to a multi-core cable. Normally, a constant spacing between adjacent electrodes is used. The multi-core cable is attached to an electronic switching unit which is connected to a laptop computer. The sequence of measurements to take, the type of array to use and other survey parameters (such the current to use) is normally entered into a text file which can be read by a computer program in a laptop computer. After reading the control file, the computer program then automatically selects the appropriate electrodes for each measurement. One technique used to extend horizontally length covered of the survey, particularly for a system with a limited number of

electrodes, is the roll along method (Figure 3.4). After completing the main sequence of measurements, one of cable is moved to the end of the line.

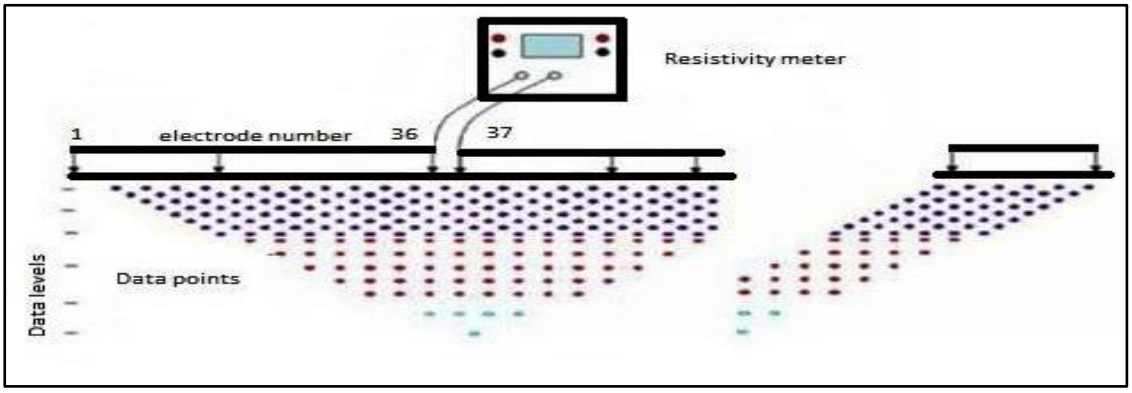

Figure 3. 4 Generalized survey procedures with the main sequence in the left, rollalong in the right and data points of 2-D resistivity imaging (Tigistu Haile, 2010).

3.1.4.3 Modeling of 2-D electrical resistivity imaging

Resistivity data is generally interpreted using the modeling process. A hypothetical model of the Earth and its geo-electrical section is generated. The theoretical electrical resistivity response over that model is then calculated. The theoretical response is then comparing with the observed field response and difference between the observed and calculated are noted. The hypothetical earth model is then adjusted to create a response with more fit to the observed data.

a) Forward modeling

Forward modeling is a method to model a subsurface by estimating the actual resistivity of the different geological structures. The estimation is made by calculating the apparent resistivity of the respective ground structure using the fundamental theoretical electrical equations. The program calculates the apparent resistivity from the recorded current and potential. It then processes and constructs electrical pseudo section of 2-D subsurface model. The forward modeling is achieved by a program that works by dividing the subsurface into a large number of small rectangular cells.

b) Inverse modeling

Geophysical data inversion is a method designed to find a model that gives rise to a parameter similar to the actual measured parameters or data. The model is an idealized mathematical representation of a section of a subsurface earth, having a set of model

parameters that are the physical quantities estimated from the observed data. The instrument measures the apparent resistivity of the subsurface materials. This is not the true resistivity of the sub surface materials. The relationship between the apparent resistivity and the true resistivity is a complex relationship. The complex mathematical formulation required to determine the true subsurface resistivity from the apparent resistivity values is inversion problem. A program developed to solve this problem is referred to as an inversion program. The optimization method basically tries to reduce the difference between the calculated and measured apparent resistivity values by adjusting the resistivity of the model blocks. A measure of this difference is given by the root-mean squared (RMS) error. However, the model with the lowest possible RMS error can sometimes show large and unrealistic variations in the model resistivity values and might not always be the "best" model from a geological perspective. In general the most prudent approach is to choose the model at the iteration after which the RMS error does not change significantly. This usually occurs between the 3^{rd} and 5^{th} iterations. The root mean squared (RMS) error equation given as

$$e = \sum_i^n \left(\sqrt{(m_i - r_i)^2} \right) \tag{3.32}$$

Where r_i is the i^{th}calculated (model response) resistivity value, m_i stands for i^{th}observed or input apparent resistivity, *n* is the number of measured data. In matrix form, taking all and each and their difference (let as column vectors; *r, m* and *g* and rearranging the above equation can be formulated for square error function as

$$e = \sum_{i=1}^n g^2 = g^T g \tag{3.33}$$

Vector *g,* that is the difference between the observed and the model response is called discrepancy vector. To get the minimum RMS error the smoothness constrained least-squares method (DeGroot-Hedlin and Constable, 1990; Sasaki 1992) is used. The smoothness-constrained least-squares method is based on the following equation.

$$\left(J^T J + U.F\right)d = J^T g \tag{3.34}$$

where, $F = f_x f_x^T + f_z f_z^T$, f_x = horizontal flatness filter, f_z = vertical flatness filter, J = matrix of partial derivatives, U = damping factor, d = model perturbation factor and g = discrepancy vector.

3.2 Seismic methods

3.2.1 Introduction

Seismic measurements are well known from their use in hydrocarbon exploration, but can also be applied for mapping of shallower underground structures such as buried valleys. Seismic waves are created by a hit on the surface and they travel underground. Like sound waves, they are reflected and refracted when they reach a boundary between different layers in the underground. Using the time required for the wave to come back to the surface and the velocity of travel, we can determine the depth of different geological boundaries. The velocity value of the waves carries information on the type of sediment or rock. This method is important not only for structural information, e.g. in delineating faults or valley structures, but also for physical characterization of layers and thus is very useful in hydrogeological investigations. Since the 1920's, seismic reflection techniques have been used to search for petroleum and refraction techniques have been used in engineering applications. Additionally, since the 1980's, significant strides have been made in both near-surface seismic reflection surveying and in the development of shallow-seismic refraction methods.

Near-surface methods use an adaptation of parameters to high resolution information – that is the capacity to discriminate layers – and may provide results also from layers that are 500 m in depth, such as deep buried valleys.

3.2.2 Physical background

Seismic waves include body waves that travel three-dimensionally through solid earth volumes and surface waves that travel near the surface of the earth volume (Fig3.4.). Surface waves are categorized further as Love waves and Rayleigh waves; the ground roll e.g., is a Rayleigh wave. For seismic investigation of the ground, the use of body waves is standard. Here

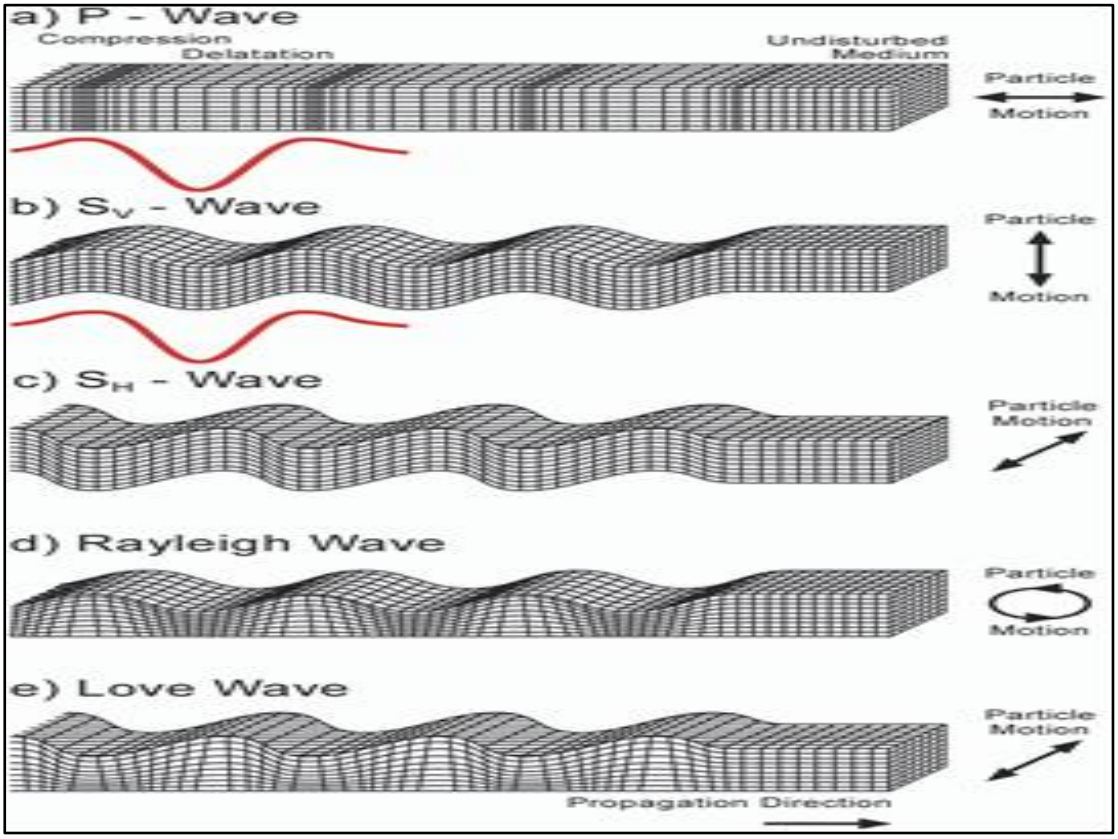

Figure 3. 5 Types of seismic waves

we have to differ between compressional waves (P-waves) and shear waves (S-waves); the difference is in the particle motion of the wave propagating through the underground material. The velocities of these waves depend on the elasticity and density of the underground material and can be expressed by:

$$V_p = \sqrt{\frac{k + \frac{4\mu}{3}}{\rho}} \tag{3.35}$$

$$V_S = \sqrt{\frac{\mu}{\rho}} \tag{3.36}$$

With the elastic constants k (= bulk modulus) and μ (= shear modulus) and the mass density ρ of the material through which the wave is propagating.

For unconsolidated sediments like gravel, sand, or clay, P-wave velocities range from 200 – 800 m/s for dry, and 1500 – 2500 m/s for water- saturated material. S-wave velocities are much slower, in the range of 100 – 500m/s, and do not differ between dry and water-

saturated material. Due to its slowness, the S-wave arrives later than the P-wave and is named secondary (S) wave in contrast to the primary (P) wave.

In sedimentary material, elasticity and density strongly depend on porosity. At a layer boundary, e.g. between sand and clay or till, a porosity change normally occurs, leading to contrasting densities and seismic velocities. A seismic wave impinging on this layer boundary will be partly reflected and partly refracted (Fig 3.5). The intensity of the reflected wave depends on the magnitude of the contrast between seismic velocities and densities at the boundary, regardless of the sign of the contrast. The product of velocity V and density ρ is the acoustic impedance I = V ρ of a medium. The strength of a reflection from an acoustic contrast interface is defined by the reflection coefficient

$$R = \frac{I_2 - I_i}{I_1 + I_2} \tag{3.37}$$

With I_1 = acoustic impedance of the first layer and I_2 = acoustic impedance of the second layer. Equation 3.37 is valid for normal incident rays or waves (ray path perpendicular to layer boundary).

The discussion of seismic waves can be in terms of wave fronts or ray paths, the latter being a line perpendicular to the wave fronts. The energy of a seismic wave is proportional to the square of its amplitude. An important relation of frequency to space and time is the wavelength (λ), which describes the distance in space between successive peaks (or troughs) of the seismic wave and restricts seismic resolution, i.e. the capacity to discriminate layers. Layers with thickness less than λ/4 are not resolvable with the seismic reflection method. The propagation velocity (V) of a wave is the product of its frequency (f) and wavelength: V = f λ. As V is a physical property intrinsic to the material, in seismic data, higher frequencies result in shorter wavelength and better resolution.

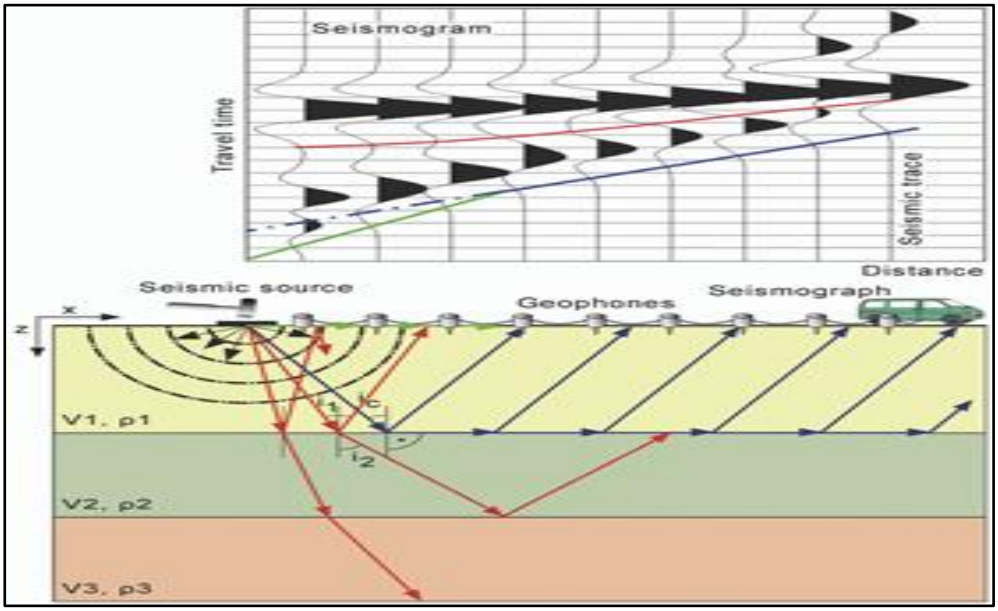

Figure 3. 6 Sketch of seismic survey: layer model, seismic rays and resulting seismogram with appropriate seismic signals.

For geometrical ray propagation the fundamentals of optics are valid, e.g. Fermat's principle of least-time path and Snell's law, describing how the wave changes direction when crossing the boundary between media one and two:

$$\frac{\sin(i_1)}{v_1} = \frac{\sin(i_2)}{v_2} \tag{3.38}$$

with I_1, I_2 angles of incidence and V1, V2 velocities of the media. A special type of wave propagation occurs at layer boundaries with increasing seismic velocities (V2 > V1). At an angle of incidence called critical angle (I_c; sin i_c = V 1 V2) the (critically) refracted wave front propagates along the interface rather than into the medium itself. This is the head wave used in the refraction seismic method. For the reflection seismic method, rays with angles of incidence less than the critical angle are usually used, allowing transmission into the next medium; with angles of incidence larger than the critical angle, total reflection occurs with the effect of relatively strong amplitudes. Both reflected and refracted waves can be recorded at the surface and their travel times can be measured and used for detection of underground structures.

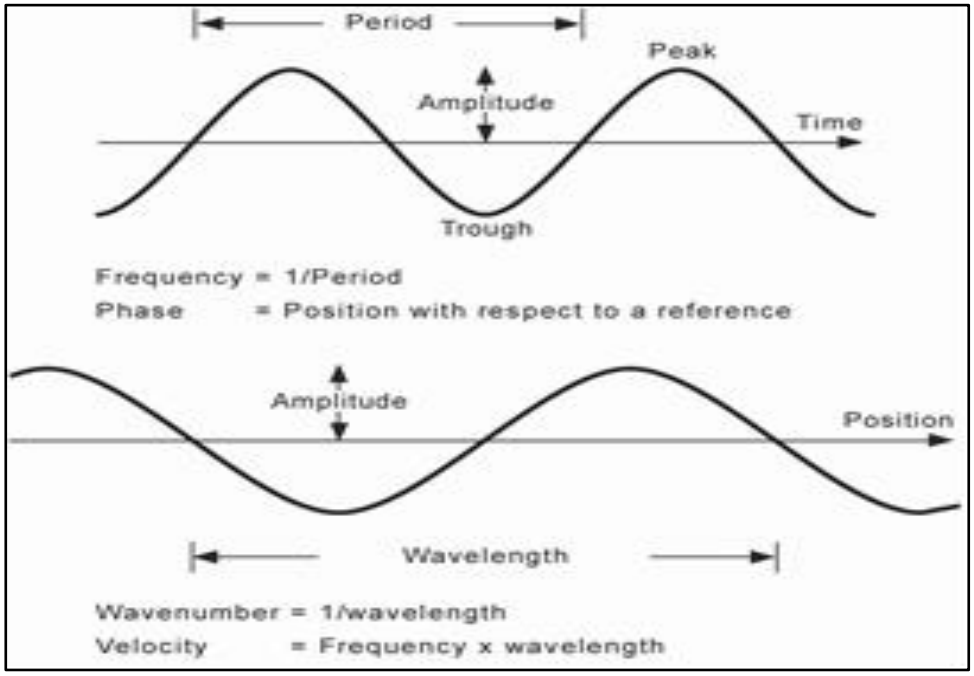

Figure 3. 7 Wave definitions for sinusoids: a) how displacement varies at a particular location with time, b) how a wave looks at different places at a given instant (after Sheriff 2002)

3.2.3 Seismic measurements

Depending on the travel path of the seismic wave, we differentiate between the seismic refraction method and the seismic reflection method.

A special feature of the refracted or head wave is that it travels along the interface with the velocity of the higher speed medium. Remember that this wave is only created if the velocity on the underside of an interface is greater than in the overlying layer. Therefore, the wave can travel faster than reflections in the overlying medium, which results in it being the first arrival in the seismogram. This is valid at least from a critical offset that is dependent on the critical angle. Being restricted to geologic conditions of increasing seismic velocity with depth, this method alone is not recommended for buried valleys that are incised in sedimentary surroundings with similar physical parameters relative to the valley fill itself. Here the reflection seismic method is adequate and offers much more details.

Reflections, which arrive later than the refractions in the seismogram, successively give the images of layer boundaries in depth or seismic travel time. The depth of penetration is limited by the energy of the seismic source and loss of energy through attenuation in the

earth material. A reflection seismic measurement includes the near-surface refracted signals as first arrivals. These are interpreted for the very near-surface velocity and depth model and so may complement the seismic reflection interpretation that usually lacks information for the very near-surface area (e.g. 2 to 10 meters). This model is also used for static corrections.

The aim of seismic reflection measurements is a zero-offset seismic section where source and receiver points coincide; this presents the image of a geologic cross section or depth section of geologic boundaries and is what an echo sounder usually yields. As a field technique the common midpoint method is established (CMP method; Fig.3.7). The basic idea is that a subsurface point is covered by several rays or waves with different angles of incidence or different shot-receiver offsets. Presupposing horizontally layering, this subsurface point is graphically the midpoint between shot and receiver location. The number of rays or waves covering the subsurface point is known as fold or coverage. By using different offsets of this so-called CMP gather and the different arrival times for a reflection, the velocity of the subsurface medium can be derived. With this velocity, the traces are corrected to zero- offset and stacked to a single trace (Fig3.8). The advantage of the CMP method in regard to a single fold zero-offset measurement is the derivation of seismic velocities and an improved signal/noise ratio by the multi fold coverage. In practice, a shot is recorded by several receivers with different offsets and this arrangement is moved successively. In a later data processing step, the traces belonging to one CMP are sorted from the shot gathers. The (in-line) coordinates X_{CMP} of CMP, X_S of source and X_G of receiver location are related to each other by:

$$X_{CMP} = \frac{(X_S + X_G)}{2} \tag{3.39}$$

The CMP spacing is half of the receiver interval. The fold of the CMP (N_{CMP}) is given by the receiver spread length (= number of receivers N_G times receiver interval ΔX_G) and the shot interval ΔX_S

$$N_{CMP} = N_G \times \frac{\Delta X_G}{(2\Delta X_S)} \tag{3.40}$$

The interpretation of the seismic reflection section can be much improved by borehole information. The data are linked by a vertical seismic profile (VSP) that allows the accurate determination of the travel time from the surface to various geologic units.

3.2.4 Field techniques

For the field layout of a seismic survey, independent of reflection or refraction, we need a seismic source; several seismic receivers (geophones) connected by cable, and connected to the seismograph. Usually the survey will be done along profiles determined by logistics and costs but 3D information should be the optimum. The equipment and configuration have to be adapted to what we are investigating to make sure to get the best quality data possible for the given objective.

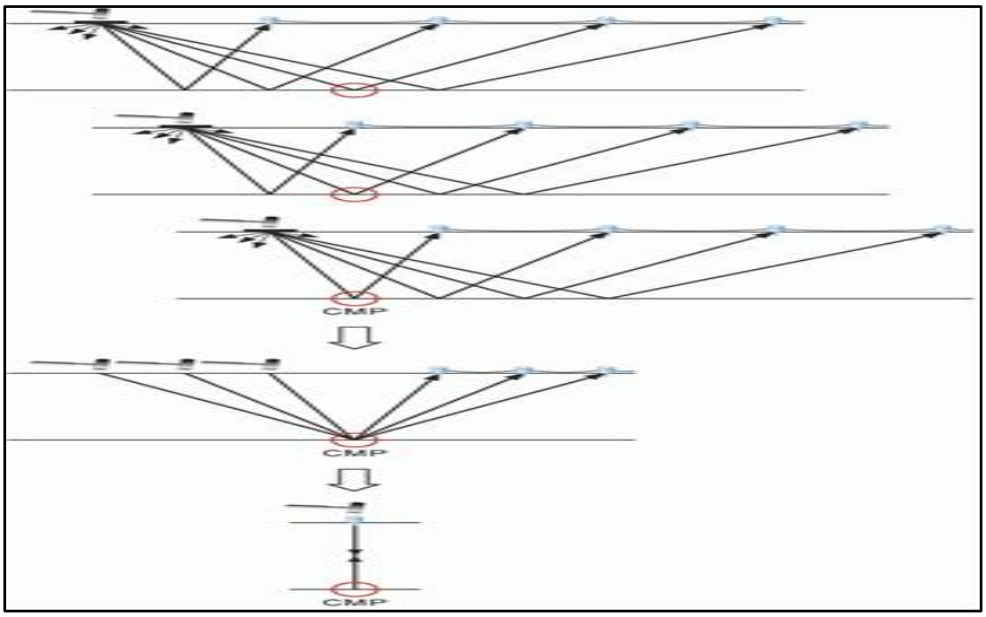

Figure 3. 8 Sketch rays for common midpoint (CMP) method

3.2.5 Field acquisition parameter design

Proper configuration of the field parameters is essential for the success of the seismic survey. Among the important field parameters are geophone spacing, shot spacing, and shot point offset to the geophone. It is important to consider carefully what it is that we want to see. A simple model including travel time curves for the key reflectors and the expected arrival times of coherent noise, like ground roll or surface waves and air-coupled waves, may be very helpful and may be calculated by simple formulas. This is done for the case of a buried valley in sedimentary environment. The result is shown in Figure 3.9.

Direct waves, surface waves (ground roll), or air- coupled waves start travelling from time zero, that is with triggering the shot, and proceed directly to the receivers at distance x with generally relatively low velocity V (and low frequency and high amplitude). The travel time is

$$t_{direcg} = \frac{X}{V} \tag{3.40}$$

These waves are "noise" – that is unwanted signals – in a seismic reflection survey and form a so-called "noise cone" (Fig. 3.8).

$$t_{refracted} = \frac{X}{V_2} + \frac{2Z}{V_2}\sqrt{\left(\frac{V_2}{V_1}\right) - 1} \tag{3.41}$$

with thickness z of the first layer.

Reflected waves are not restricted to velocity increase but are generated at any interface in the subsoil where the density or velocity changes discontinuously. The arrival time of the reflection at the surface will always be later than the refracted wave from the same interface or at most tangent to the refracted travel time. The travel time can be evaluated by

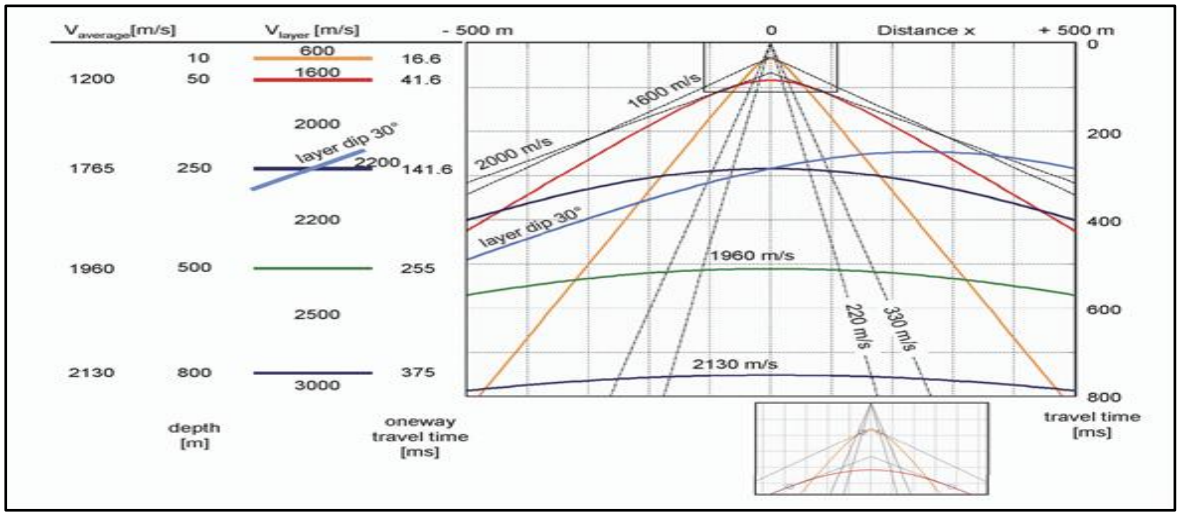

Figure 3. 9 Velocity-depth model and appropriate travel time-distance model of expected seismic response and coherent noise.

$$t_{reflected} = \frac{1}{V}\sqrt{X^2 + 4Z^2} \tag{3.42}$$

This gives the shape of a symmetrical hyperbola in the travel time-distance plot or, considering a layer dip of angle δ from the horizontal a hyperbola where the apex is displaced from the centre:

$$t_{reflected} = \frac{1}{V}\sqrt{X^2 + 4Z^2 + 4XZ + (\sin\delta)} \tag{3.43}$$

For the multilayer case, for this simple calculation the average velocityV_{ave}, calculated from interval velocities V_i and thickness Z_i of the i layers (travel time across each layer is $t_i = \frac{X_i}{V_i}$) should be used:

$$V_{average} = \frac{\sum_i Z_i}{\sum_i \frac{Z_i}{V_i}} \tag{3.44}$$

or the root mean square velocity V_{rms} which is more equivalent to the normal move out velocity V_{NMO} that we need later for dynamic corrections:

$$V_{rms} = \sum_i \frac{V_i^2 t}{\sum_i t_i} \tag{3.45}$$

RMS velocities are typically a few present larger than corresponding average velocities due to the specific travel paths.

For the design of field parameters and to best record the reflected wave field the maximum and the minimum offset must be defined. The maximum offset should be as large as possible to aid velocity analysis. At the same time, it must be small enough to avoid wide angle reflection distortion (reflections with angle of incidence near or greater the critical angle). It must also be small enough so that the most important reflection arrives just below the mute zone applied during processing. A rule of thumb is to set maximum offset equal to the depth to the deepest target reflector. Another point to keep in mind is that many seismic sources generate noise (like ground roll etc.) with large amplitudes that superpose the reflection energy in the noise cone (see also Fig. 3.8).

Often, filtering of the noise is a problem and one has to mute, or zero, this part of the data during processing.

The minimum offset should be close to zero. On one side we then have control for velocity and timing. On the other side it is useful to have first arrival (refraction) information near the source for static and datum correction. When minimum offset becomes too large these events are not recorded. Near-surface reflections are often difficult to record because of the noise cone. The geophone interval is a function of maximum offset, minimum offset, and number of traces available in the seismograph, the required spatial sampling, and the spatial resolution. The latter are the most important to consider. A strict criterion for the reconstruction of a wave field is that there must be two or more samples per cycle for the highest frequency present (Nyquist theorem). This determines the sampling interval of the time series recorded at a fixed position, i.e. the geophone, as well as the wave at different places at a given instant, i.e. the spatial sampling interval or the spacing of the geophones. To make this clearer, look at the wavelength definitions in Figure 3.9.

The apparent surface wavelength is a function of emergent angle of the seismic ray. Surface waves propagating horizontally along the ground have an apparent surface wavelength equal to their true wavelength. The shallowly emergent reflected signal has an apparent surface wavelength greater than its true wavelength, but less than the apparent surface wavelength of more steeply emergent reflected energy. In general, apparent surface wavelength λ_a is true wavelength λ divided by the sine of the angle of emergence Θ: $\lambda_a = \lambda / \sin \Theta$. For vertically incident rays ($\sin\Theta=0$), the apparent surface wavelength is infinite; this concerns most reflected signals so the above considerations are not as critical for reflections from horizontal layers, but for dipping layer reflections. Thus for the proper spatial sampling of a reflection from a dipping reflector the geophone spacing Δx must be less than half the projection of the shortest wavelength onto the surface. That is

$$\Delta X_{\max} \le 0.5 \frac{\lambda_{\min}}{\sin \delta} = \frac{0.5 V_{avg} / f_{\max}}{\sin \delta} \qquad (3.46)$$

with δ maximum dip of reflector.

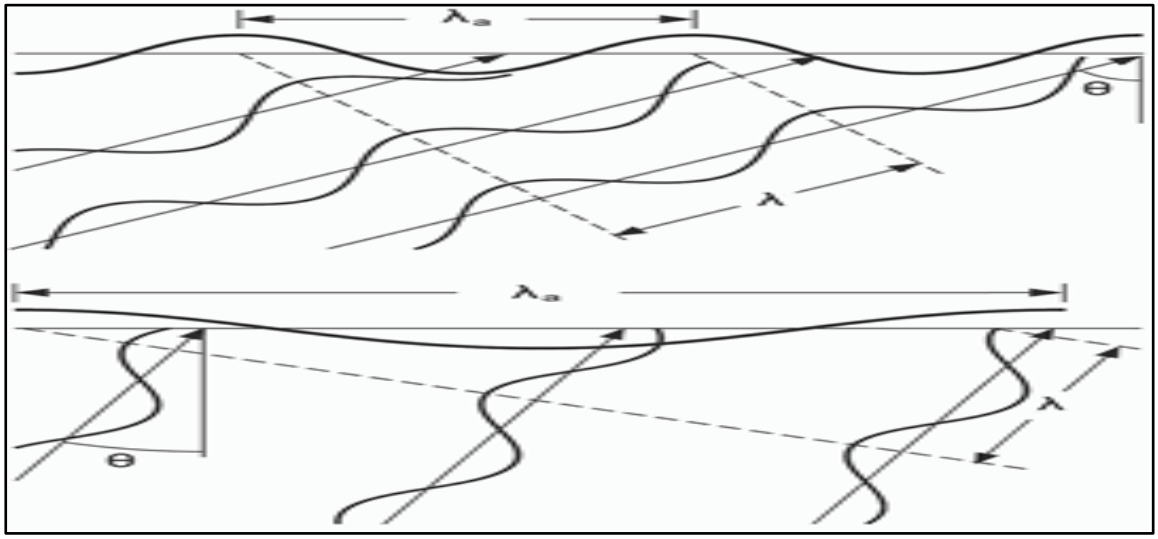

Figure 3. 10 Apparent surface wavelength versus angle of emergence

From the reflection signal point of view, another consideration in determining receiver interval involves the concept of the first Fresnel zone. Reflected energy represents a sampling from a relatively large area of the reflecting surface and this is related to the first Fresnel zone. The size and shape of the first Fresnel zone depend upon reflector depth Z and wavelength λ of the reflected energy:

$$R = \sqrt{\frac{Z\lambda}{2}} = 0.5V\sqrt{\frac{T_0}{f}} \tag{3.47}$$

with R the radius of the first Fresnel zone, V velocity and T_o two-way traveltime. If T_o = 0.1 s, V = 1600 m/s and f = 150 Hz, the size of the first Fresnel zone is 40 m. This is roughly the size of the reflecting "point". With a receiver interval including at least 2 traces (that are 4 CMPs) per Fresnel zone, the reflector is well sampled. Spatial considerations can also be used to attenuate or to improve waves by grouping geophones or shots in special arrays. In exploration seismology, linear arrays are used to attenuate the ground roll that usually is characterized by relatively low velocity, low frequency, and high amplitude. Arrays start to attenuate signals when their length is a quarter of the apparent surface wavelength and larger (Fig.3.10).Thus to attenuate the unwanted ground roll that has a relatively large wavelength, the array also must be relatively large. On the other hand, to enhance reflection signals of possibly high frequency, the array length may not be larger than a quarter of their apparent surface wavelength. Therefore the array length should in no case be larger then

$$L_{\max} \le 0.25 \frac{V}{f_{\max}} \sqrt{1+4\frac{Z^2}{X_{\max}{}^2}} \tag{3.48}$$

with z the depth to the shallowest reflector, $X_{max}$the maximum source-receiver offset, $f_{max}$the highest frequency contained in the reflection signal, V the average velocity to the reflector and L_{max} the maximum array length. If we accept as a rule of thumb that the maximum source-receiver offset is roughly equal to the target depth for reflected energy that is not a wide-angle reflection, then the following equation can be used:

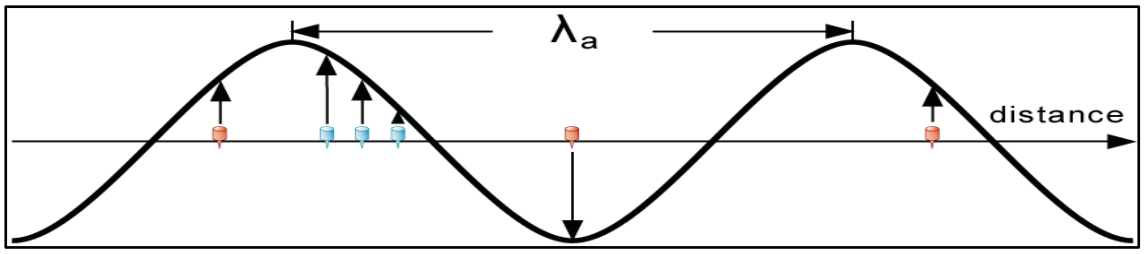

Figure 3. 11 Geophone array response versus apparent surface length λ_a.

$$L_{\max} \le \frac{0.5V}{f_{\max}} \tag{3.49}$$

In shallow, high-resolution reflection seismology, arrays cannot be effectively employed to attenuate ground roll. Now to answer the question where to place the shot in the active geophone line: it is always preferable to use a symmetrical split-spread with the geophones evenly split on either side of the source. When the number of data channels available is not sufficient, end-on geometry with the source on one side of the geophone line is used to get the offset required for the target reflection (the sketch in Fig. 3.4 shows end-on geometry). When reflections from dipping horizons are expected, preferred end-on geometry is that where the geophones are placed up dip from the source. Additionally, one must consider the record time length, that is the least time needed to record the reflection from the deepest target horizon; e.g., if the depth z of the buried valley is 400 m and an average velocity V of 2000 m/s for the sedimentary fill can be assumed, then the reflection time t of the valley base would be t = 2z / v and thus be 400 ms or 0.4 s. This is the two-way reflection time. To image also the surrounding or geological setting, the recording time in this case should be 1s. If we want to look deeper, we would have to

raise this time value. For a proper sampling of a cycle, at least two samples are necessary. Expressed in relation to frequency, this means that the highest frequency that can be resolved, the Nyquist frequency f_{Ny}, needs the time between two sample points or sampling interval to be $\Delta t = 1/ 2f_{Ny}$ with Δt in milliseconds (ms) and f in hertz (Hz). In practice, four samples are recommended, $\Delta t = \frac{1}{4 f_{Ny}}$ of Example: with a sampling interval of 1 ms, frequencies up to 250 Hz are well sampled; the Nyquist frequency is 500 Hz. To avoid aliasing, frequencies above the Nyquist frequency must be removed before sampling. The inverse of the sample interval is called sample rate $\left(\frac{1}{\Delta t}\right)$.

CHAPTER FOUR

4. DATA ACQUISITION, PROCESSING AND PRESENTATION

4.1 Electrical Resistivity of 2-D Imaging

4.1.1 Instrumentation and Data Acquisition

The electrical resistivity data was collected using the IRIS instruments SYSCAL R1 plus Switch 72 multi-electrode resistivity meter that uses 72 electrodes working in "multi-electrode" mode, through inter connectable four reel cables accepting 18 electrodes each, 72 short connector wires and two movable connector boxes (Figure 4.1). The cables used in the particular instrumentation have pick up/connection points spaced at 5m. The instrument records automatically with the format uploaded into the unit and the system takes measurements almost individually once the array are laid along the profile by selecting four relevant electrodes according to the array type.

Figure 4. 1 Instrumentation of 2-D electrical imaging.

Reel cables are interconnected each other with connector boxes and each cable outlet is joined to electrode by the connector wires. A twelve volt external battery was used for this survey. In the survey, the instrument is usually placed at the midpoint, where the deepest depth is recorded, and the four cables reels spread on both side of the resistivity

meter. The two cables are in one side of the resistivity meter while the other two are spread on the other side of the resistivity meter (Figure 4.2).

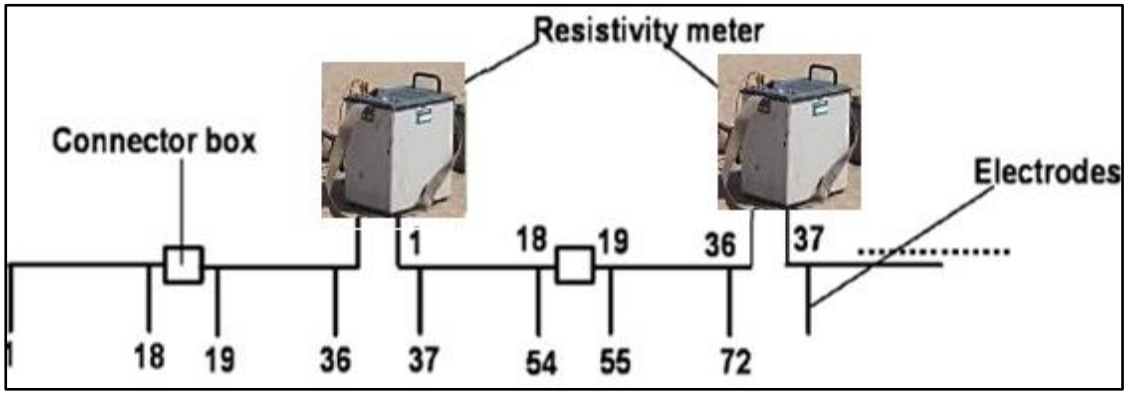

Figure 4. 2 General field layout of 2-D electrical imaging.

The instrument allows the recording of accurate and reliable measurements through the high power and high sensitivity characteristics. 5m electrode spacing was chosen for all surveys in order to achieve high spatial resolution data to the practically acceptable depth of up to 68 to 70 m and was made with the mixed Wenner – Schlumberger multi electrode array configuration. A total of ten profiles were surveyed and seven of these profiles were carried out at site-1, which has five parallel profiles and two transversal profiles, two crossing profiles at site-2 and one profile at site-3. Each profile except profile one which has ten rollalongs, containing one main and two rollalong sequences in order to cover the required length which is more than 500 m. The orientation of the profiles in site one is aligned from southeast to northwest direction. In addition to these, two profiles (a cross profile line) almost at right angles to the five profiles was conducted in order to detect structures potentially oriented parallel to the three profiles (Figure 4.3).At site two, two crossing ERT lines were centered on the proposed site in N-S and E-W orientation. At site 3 a single profile was acquired from the alluvial fan in to the basin in an E-W orientation.

4.1.2 Data Processing and Presentation

At the time of data acquisition no work was made to filter the data; rather, once a line was finished, the ERT data was moved to the computer for additional data processing. The software Prosis II was used for various purposes like downloading the data from the instrument, join the main sequence and the number of rollalong data set, to filter the data for repeated values and to edit extremely large variation in the resistivity (typically noise

in ERT is shown by resistivity values that are two or more order of magnitude higher than average values recorded along the lines).The resulting data set was exported in the form of a ".dat" format for analysis with inversion software. The resulting apparent resistivity values were then uploaded to Res2dinv (geotomo) for modeling of apparent resistivity section using a standard gauss newton method (loke and Dahlin, 2002). The resultant 2D and 3D sections were then used for final interpretation.

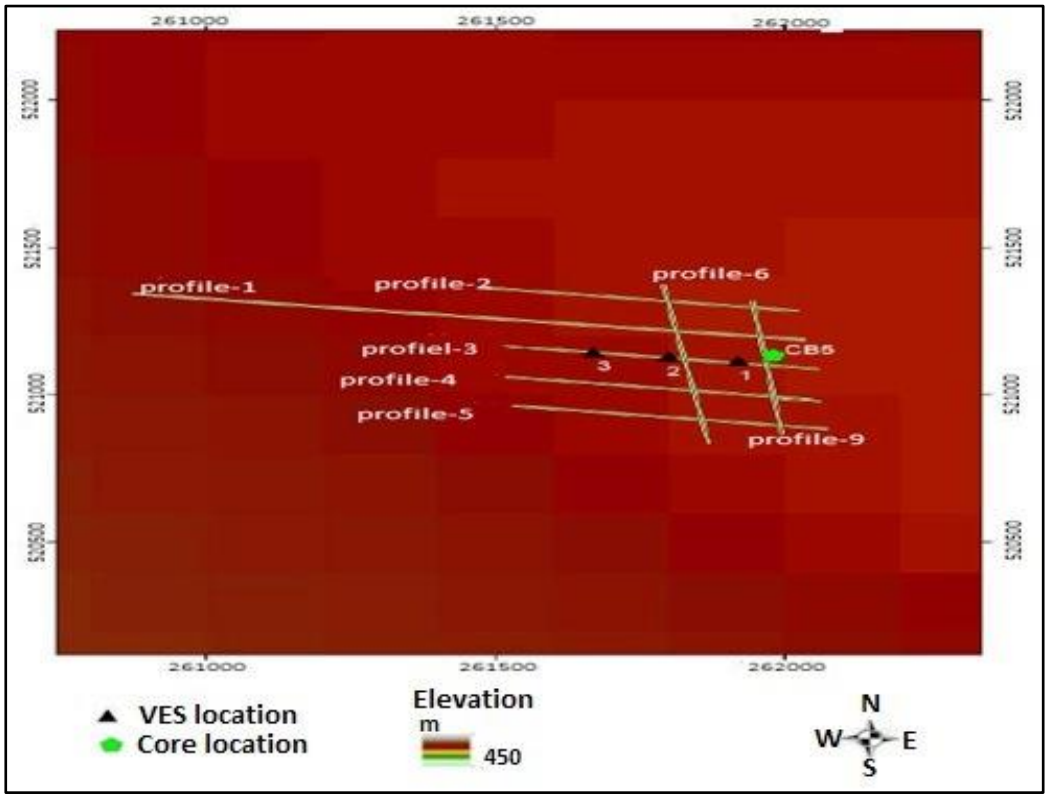

Figure 4. 3 Base map of the study area that shows site -1 of electrical 2D survey lines and previous borehole and VES points (1,2,3).

The data obtained in the prosys–II software is started from 90m for each rollalong. Because of this, the rollalong sequences were adjusted with proper distance before added to the main sequence. In the case of rollalong one the data started from 90m, so no distance adjustment is needed. The second rollalong sequence data sheet was recorded after 90 meter of the first rollalong data; it was shifted by 90 meter after getting in the Prosys-II software. This step was continued for the rest rollalong data by increasing total rollalong distance by 90 meter that means 180m to the 3rd rollalong, 270m to the 4th rollalong and 360m to the 5th rollalong. After adjusting the distance, the rollalong

sequences were added to the main sequence. Topography is not incorporated to the 2D and 3D electrical resistivity section because the project site is on flat terrain.

For the data obtained in this work, each resistivity cross-section was processed independently. Figure 4.4 shows, for example, the resistivity cross-sections prepared for Profiles-2 using the RES2DINV software. Good quality of data's was used with RMS error of less than 8.2%. Finally the results obtained from the RES2DINV were correlated with the borehole data.

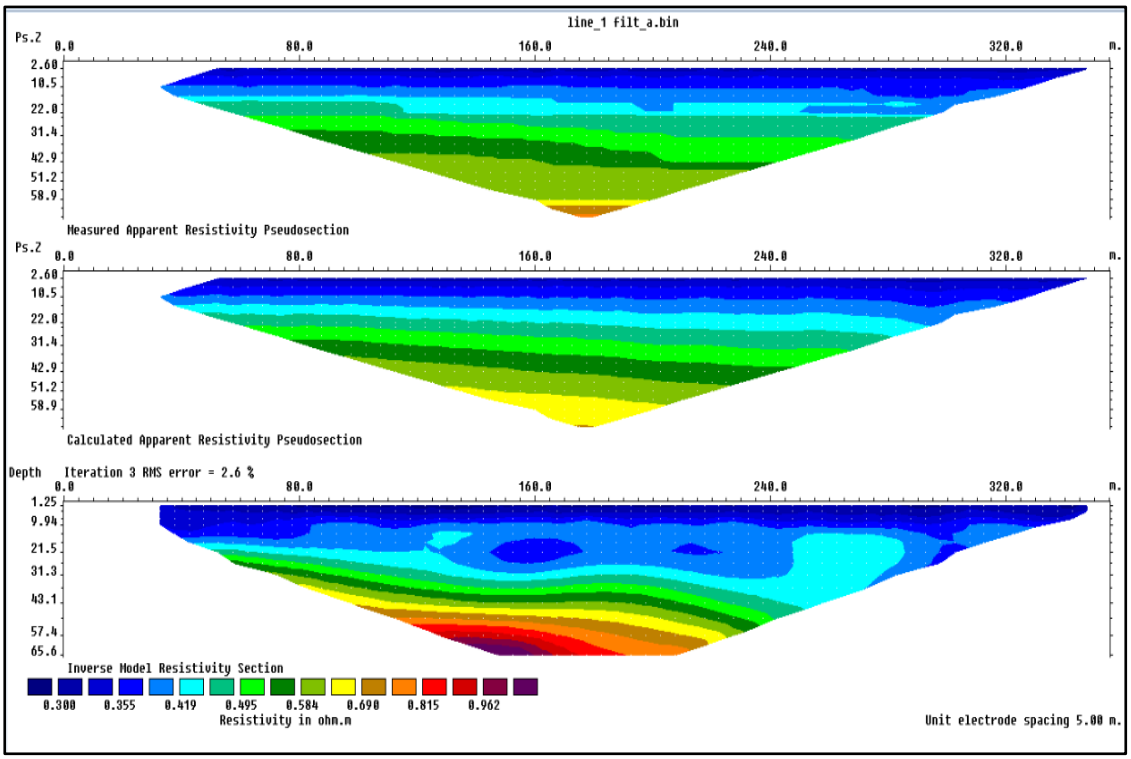

Figure 4. 4 Measured calculated and inverted apparent resistivity, and geo-electrical cross-section of Profile 2 resulting from a 2D inversion of data.

4.2 Vertical Electrical Sounding (VES) Surveys

4.2.1 Instrumentation and data acquisition

Vertical electrical soundings (VES) were acquired using the SYSCAL unit functioning in "Rho mode" with 4 electrodes arranged in a Schlumberger electrode arrangement. The maximum current electrode separation, (AB/2) =1000m, was chosen based on the depth of interest, (even if we cannot acquire the anticipated depth due to the very conductive nature of the subsurface) and subsurface geology. Long-uniform distance spacing was

used for the electrodes with maximum current electrode spacing to 2 km so electrode spacing was measured in the field using handheld Garmin GPS and pre-determined markings on the electrical cable. Three VES locations were selected, spread out along the center of the ERT grid on profile 3. The results of the VES apparent resistivity values with increased spacing were input to both the IPI2WIN and WinResist for inversion to apparent resistivity depth 1D soundings. These are presented as both layered earth models and as smooth resistivity gradient models together with their equivalence analysis.

4.2.2 Vertical Electrical Sounding (VES) data processing

After the field data have been collected, the raw resistivity data were entered to the excel sheet and arranged for other software. The apparent resistivity pseudo-depth section along the profile was prepared by using surfer-8 software. The one dimensional (1D) modeling of VES data was done by using resistivity modeling software called IPI2WIN and WinResist. The depth and resistivity of subsurface rocks beneath VES points were determined from the one dimensional inversion of VES data. The parameters from the modeled VES (resistivity and depth) are used to make the geoelectric sections along the survey lines by using Mapinfo software and later modified by AutoCAD drawing software.

4.2.4 Ambiguities of Sounding Curve Interpretation.

The Vertical electrical sounding curve modeling and interpretation is inextricably linked with the principle of equivalence. The principle expresses that a measured sounding curve is basically related with many physically equivalent models that may differ considerably. The VES data can be interpreted with different number of layers without any preference.

Another important property of vertical electrical sounding curves is evident. By all appearances, only the minimum number of layers can be deduced implying that thin layers are preferentially suppressed. A rule of thumb indicates that a layer becomes clearly visible in a sounding curve if its thickness is comparable to its depth of deposition (Kirsch, R., 2006). To avoid the ambiguity of equivalence in the 1D inversion of VES data and check the continuity of layers in the area, the data of the boreholes CB5 (core drilling bore hole-5) were used to fix model parameters. Once the resistivity and depth for the above mentioned VES were determined by fixing their depth from the boreholes

(lithology data) using WinResist software, the depth and resistivity of the other VES along this survey were estimated by using the principle of parameterization.

Furthermore, the resistivity parameters which were estimated from constrained and parameterized 1D inversion of VES data using IPI2-WIN software were used as initial model for WinResist software to find the final resistivity layer parameters.

The software WinResist uses iterations techniques to adjust the fitting between the observed data curve and the initial model parameters. Several reinterpretations for modeled soundings curves were performed to get better model parameters and the iteration process was finalized when the root mean square (RMS) errors was less than 5%.

CHAPTER FIVE

5. RESULTS, DISCUSSIONS AND INTERPRETATIONS

5.1 Introduction

Interpretation is made grounded on assimilation of outcomes from the 2D electrical imaging, vertical electrical sounding, previous seismic surveys and a borehole log data. A borehole dug at the vicinity of the study area by paleoenvironment reconstruction team was used to assist in the interpretation of the data. The total depth of the borehole is 20m while the depth of investigation of the 2-D electrical imaging is 65-68m so that, the correlation is made only for the 20m depth. Additionally, a correlation between the inverse model resistivity section and the seismic staked section around the vicinity was compared, which is surveyed around the survey line with the 2D electrical imaging.

This chapter includes interpretation of a series of inverse model resistivity depth sections; VES modeled sections together with the equivalence analysis, the results of the Tullow Oil plc Seismic refraction data and modeled cross-section between the three sounding locations which are established using different geophysical plotting software. The thorough interpretation of the study goes as follows:-

5.2 Results

5.2.1 Earth Resistivity Tomography (ERT) Results

The outcomes of the electrical imaging are presented as measured apparent resistivity pseudo-sections, calculated apparent resistivity pseudo-sections and inverse model resistivity sections in Appendix 4 and a series of inverse model resistivity depth sections in figures 5.1 and 5.2. Initial going over of sites 1 and 2 depict very low resistivity, generally, with values less than 1 ohm-m to maximum values of 20 ohm-m. At Site 3, resistivity values in excess of 500 ohm-m were recorded. Appendix 2 presents distinctive ranges of resistivity for common geological materials with different fluid fill content. At site 1, the electrical sections become more uniform from north to south through the site, with a small increase in resistivity with depth. Resistivity zones are elongated in the

horizontal suggesting layering. Profile 2, the most northerly line, illustrates the highest sort of resistivity variation with values greater than 15 ohm-m at the center of the profile.

The general lack of difference in resistivity values, it was primarily thought, might lead to a lack of sensitivity and accuracy in the inverted ground models. However, the general uniformity in form despite the very low range of resistivity value is remarkable.

Profile 6 and profile 9 was situated in order to link data across the site-1. The outcomes for profile 6 illustrate strong correlation with each of the West-East profiles. Cross-tie of profile 9 is practical in the shallow part of the section (above 15m depth) but ties at greater depth are not possible due to under-sampling of the West-East lines at this far eastward profile terminal. Results for Site 2 show analogous small variation in resistivity to that at Site 1 and show a strong similitude to the results from profile 2 and 9. At Site2 the intersection of profile 7 (N-S profile) and profile 8 (W-E profile) a good correlation is obtained, yet again indicating that the results reflect the actual geology and not noise within the data. The results for Site 3 show a different pattern with over three orders of magnitude variation in resistivity verified - values more than 500 ohm-m are observed at the beginning of the section on the alluvial fan. This greater range of resistivity values is shown in the presentation of results in figure 5.2. It should be noted that if such a range of values had been used for Site 1 and 2 results then at these sites little apparent resistivity variation would have been represented in the figures as all variations were less than 20 ohm-m.

Site-one

Profile-1

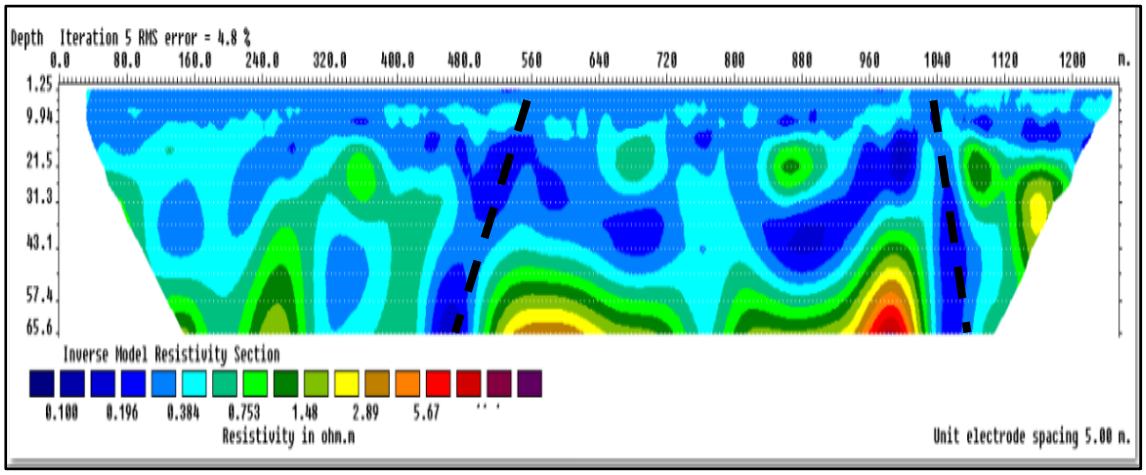

Profile-2

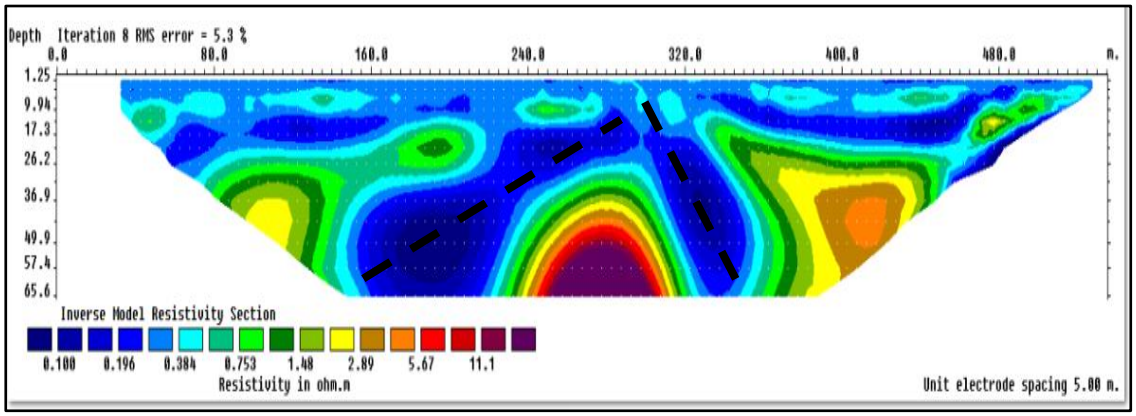

Profile-3

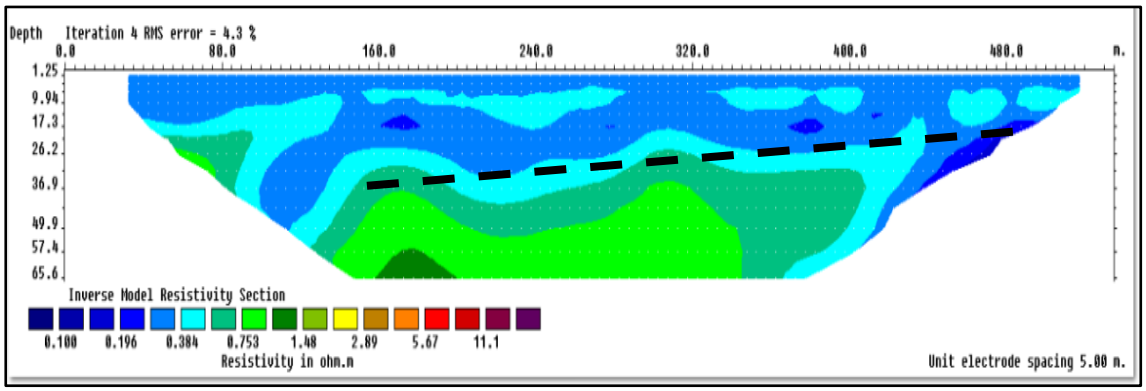

Profile-4

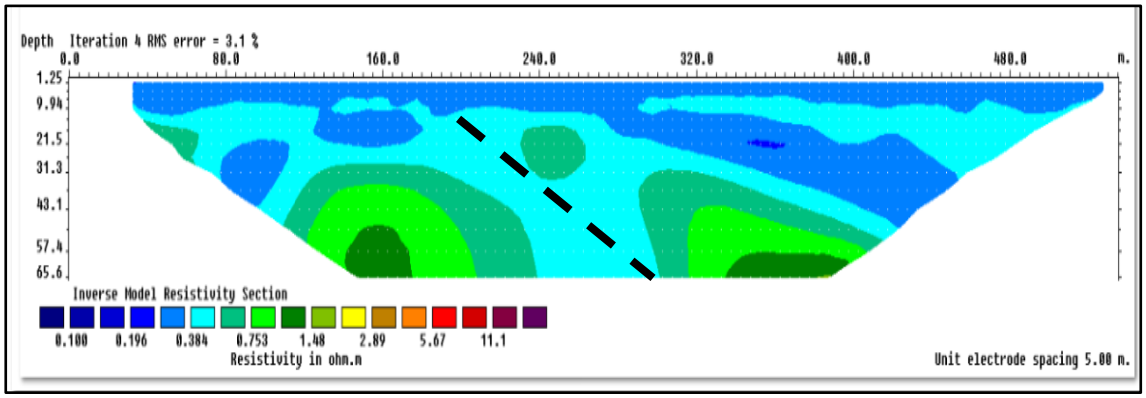

Profile-5

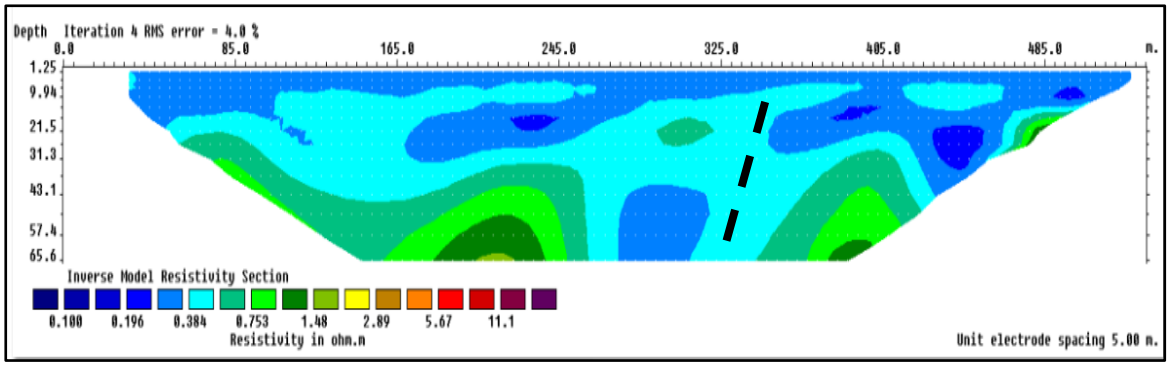

Figure 5. 1 Site 1 E-W sections showing modeled resistivity values. Note that Line1 horizontal axis is on a different scale to lines 2-5.

Profile-6

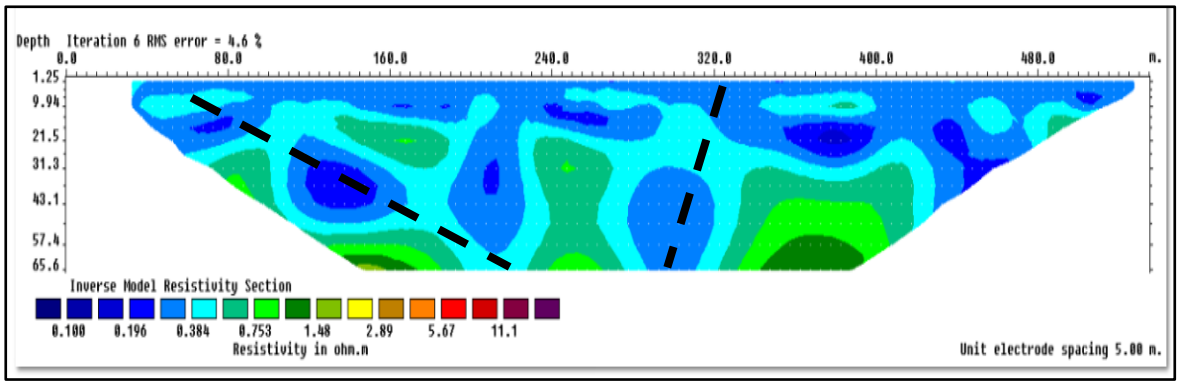

Profile-9

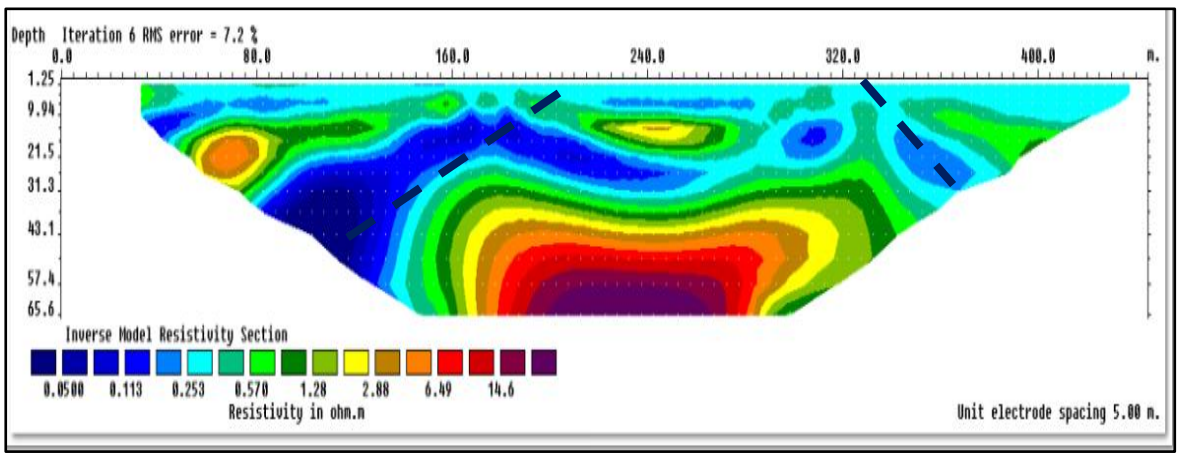

Site-two

Profile-7

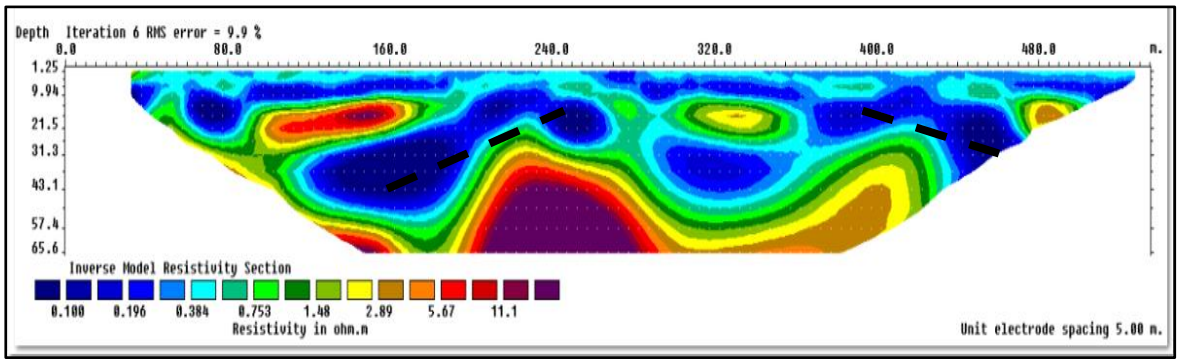

Profile-8

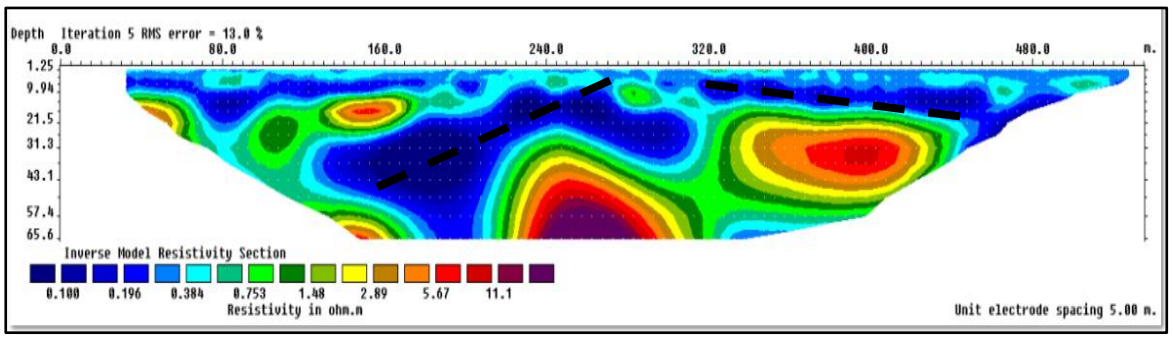

Site-three

Profile-10

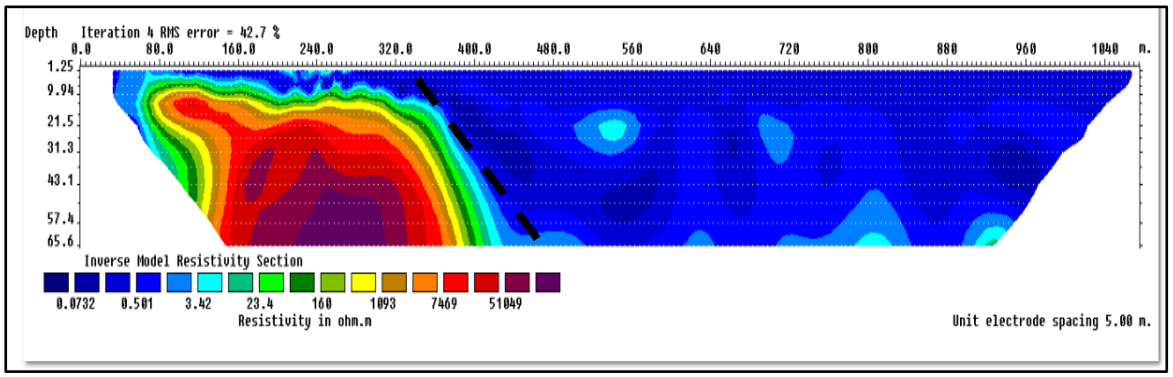

Figure 5. 2 Site 1, north-south modeled resistivity sections; Site 2, profile 7 north-south and profile 8 East-West sections; Site 3, profile 10

5.2.2 Vertical Electrical Sounding (VES) Results

The results of vertical electrical sounding (VES) modeled geo-electric sections, pseudo-sections together with the equivalence analysis are shown in figure 5.3 and 5.4.The summary for model inversion is given in table 5.1. Each model has been represented by a four or five layer earth model with a near surface conductive layer, a deeper section with relatively lower resistivity and final base layer with relatively higher resistivity. A similar overall range of resistivity was mapped to those shown with the ERT; however, the larger electrode spacing (to 1000 m) allowed for a shallow exploration depth.

Geo-electric Section

The final result from one dimensional inversion of VES data along the selected profile (profile-3) were used to construct the geoelectric sections in order to identify the distribution of different lithological units in the vertical direction. The software which were used for the inversion of the VES data were IPI2-Win and WinResist however the plotting of the geoelectric section was carried out by using Map Info and later modified by AutoCAD software. The lithological logs from boreholes that are lying on the profile were used to fix the thickness of each up to some layer by grouping the lithological units based on their type. The pseudo depth section along the survey line was examined to see the relative resistivity variations when preparing geoelectric section (figure 5.5).

The geoelectric section of profile three (figure 5.3) was constructed from the model parameters of VES points data found along profile 3 (V1-V3). The core drilling borehole (CB-5) located around the vicinity was used to constrain thickness for the layers up to some 20 m depth and later parameterize the resistivity values and depths of the other VES points using their values. The geoelectric cross-section (figure 5.3) indicates the shallow subsurface lithological units in the study area which are represented by five earth geoelectric layers (generally having small resistivity).

The major lithological units have resistivity value of the upper most layer ρ_1 (0.5-1.6), ρ_2 (0.2-0.3), ρ3 (1-2.3) and the bottom layer which can be assessed by this survey is ρ_4(0.2-21.4) and ρ5 (150-216) ohm-m are correlated to the unconsolidated sediment, silty clay, silty clay with Ca-layers, and sandy silt and sandy gravel respectively.

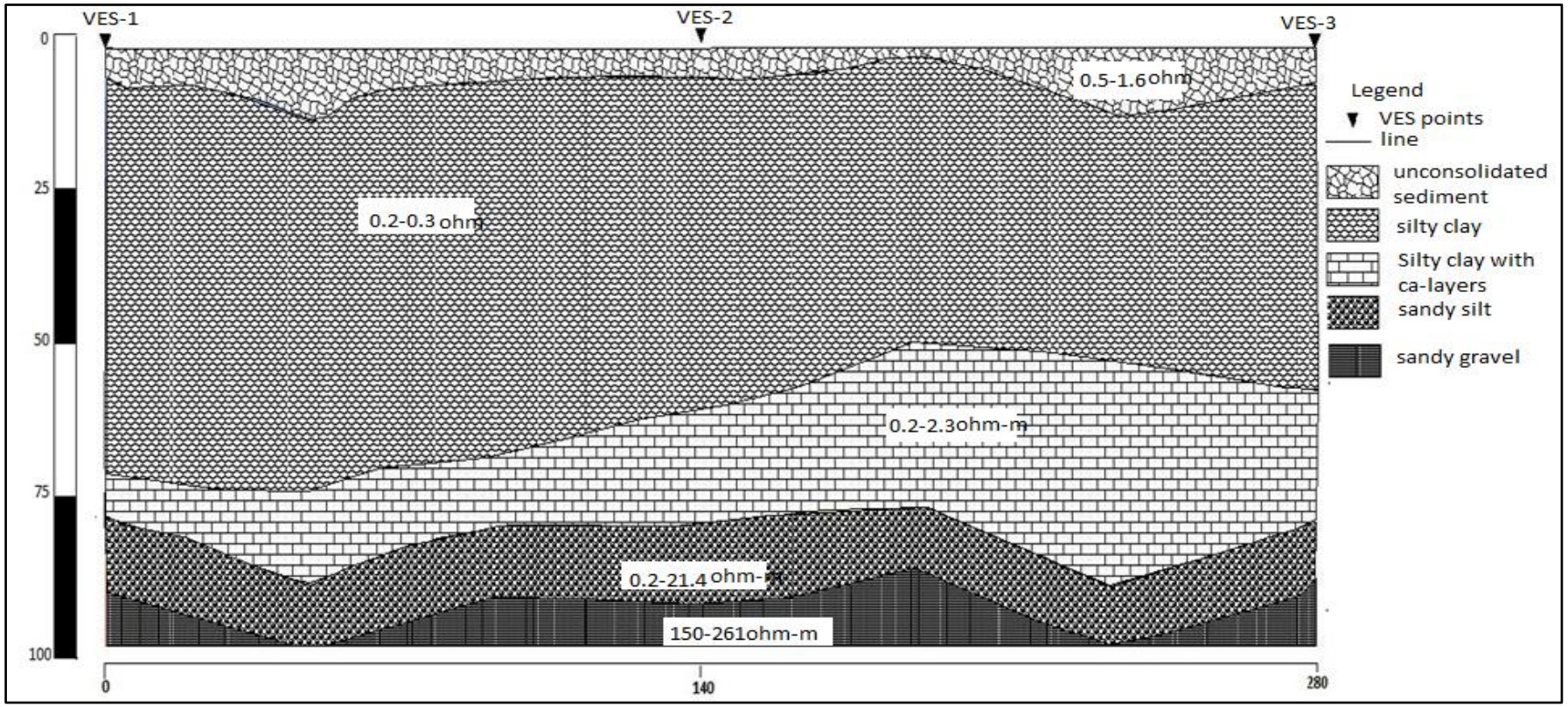

Figure 5. 3 Geoelectric section along profile-3

VES-1

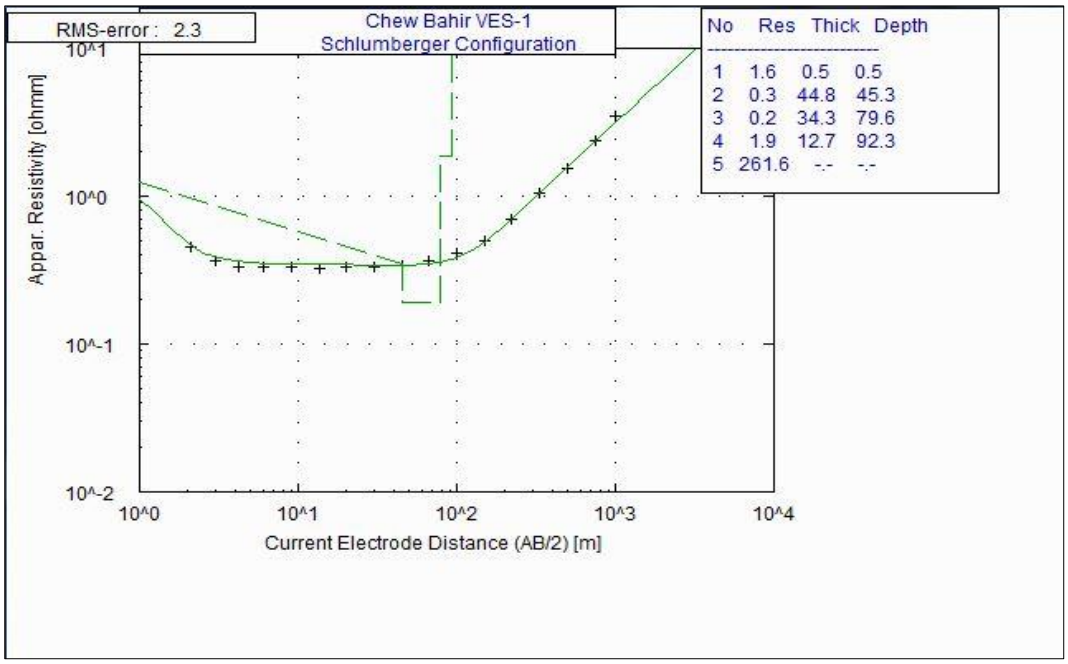
RMS-error : 2.3
Chew Bahir VES-1
Schlumberger Configuration
No Res Thick Depth
1 1.6 0.5 0.5
2 0.3 44.8 45.3
3 0.2 34.3 79.6
4 1.9 12.7 92.3
5 261.6 -.- -.-
Appar. Resistivity [ohmm]
10^1
10^0
10^-1
10^-2
10^0
10^1
10^2
10^3
10^4
Current Electrode Distance (AB/2) [m]

VES-2

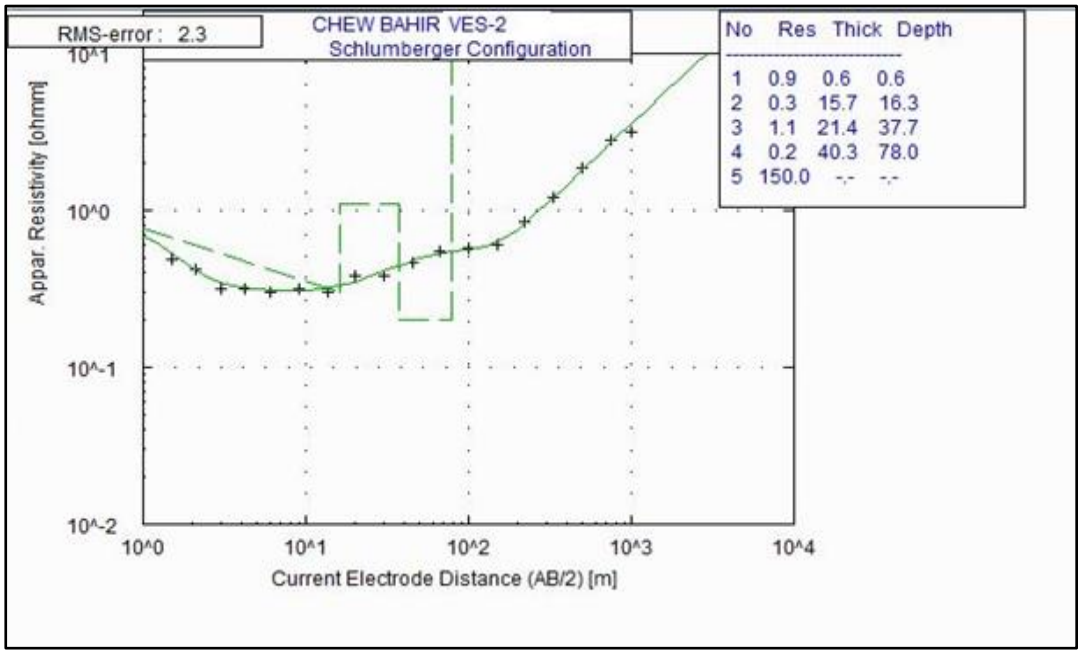
RMS-error : 2.3
CHEW BAHIR VES-2
Schlumberger Configuration
No Res Thick Depth
1 0.9 0.6 0.6
2 0.3 15.7 16.3
3 1.1 21.4 37.7
4 0.2 40.3 78.0
5 150.0 -.- -.-
Appar. Resistivity [ohmm]
10^1
10^0
10^-1
10^-2
10^0
10^1
10^2
10^3
10^4
Current Electrode Distance (AB/2) [m]

VES-3

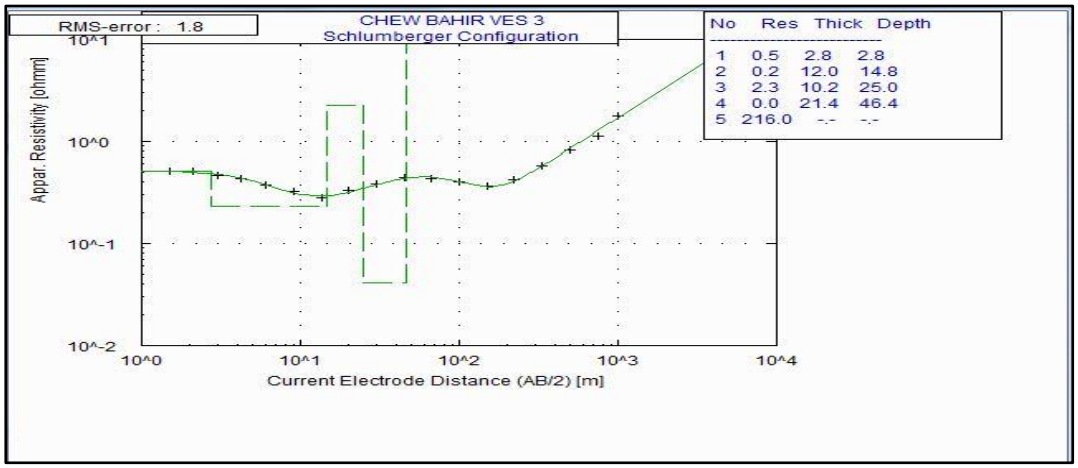

Figure 5. 4 Vertical electrical sounding (VES) models and their equivalence analysis.

Table 1. 1 Vertical Electrical Sounding (VES) models

Layer	Depth	Thickness	Resistivity
VES_1			
1	0.5	0.5	1.6
2	45.3	44.8	0.3
3	79.6	34.3	0.2
4	92.3	12.7	1.9
5	…	…	261
VES-2			
1	0.6	0.6	0.9
2	16.3	15.7	0.3
3	37.7	21.4	1.1
4	78.0	40.3	0.2
5	…	…	150
VES-3			
1	2.8	2.8	0.5
2	14.8	12.0	0.2
3	25.0	10.2	2.3
4	46.4	21.4	0.0
5	…	…	216

The results are also shown as a modeled pseudo cross-section between the three sounding locations on the figure below.

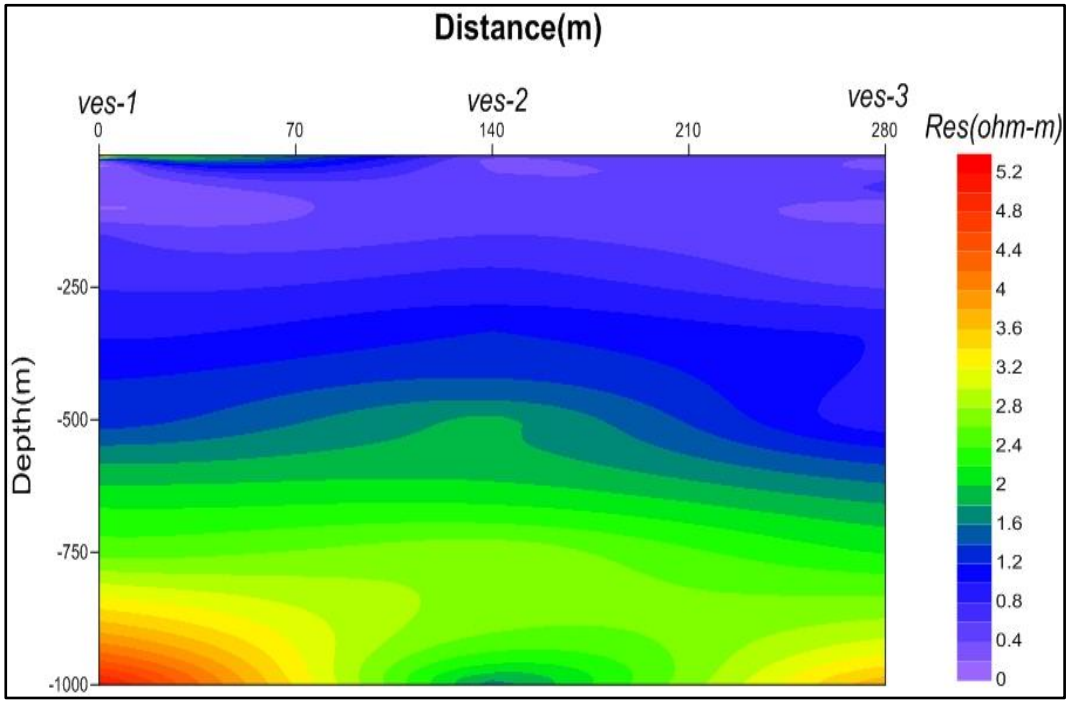

Figure 5. 5 Modeled resistivity pseudo section from vertical electrical soundings.

5.2.3 Seismic Results (after Tullow Oil plc.)

The outcomes of the Tullow Oil plc Seismic refraction data are concise in the table underneath. Two and three layer models are recommended with the near surface velocity variation between 300 and 800 m/s to depths of 12m. Below this an increase in velocity was recorded with values up to 1760 m/s. These are probably the same geological material in an unsaturated and saturated condition respectively.

Table 1. 2 Seismic velocity from refraction and uphole analysis.

Line/station	$V_1\left(\frac{m}{s}\right)$	T_1(s)	$V_2\left(\frac{m}{s}\right)$	T_2(s)	$V_3\left(\frac{m}{s}\right)$
ref57(ln13)	347	4.3	1651		
ref84 (ln21)	262	4.4	1662		
UP17	619	5.1	1465	26.16	1952
ref85(ln21)	277	7	1674		
UP14	588	13.35	1760		

Seismic reflection Line 21 is presented in Appendix 6 displayed as a brute stack in West-East orientation. The eastern basin margin is marked by a gently dipping surface from less than 100 ms two-way-time (TWT) in the East to greater than 600 ms TWT one-third of the distance into the basin. Above this gently dipping surface, near-horizontal, discontinuous reflectors are dissected in segments or blocks of generally less than 250 m length. The western end of the section does not mirror the east; rather, an abrupt discontinuity is seen in reflectors.

Seismic reflection profile 13 is presented in Appendix 6 in a south-north orientation. A gently undulating reflector dips steadily to the north across the section from depths of less than 200 ms in the south to greater than 1000 ms in the north. The reflectors are marked by their lateral continuity across the length of the section.

5.3 Discussions

The range of resistivity interpreted in both the Earth Resistivity Tomography (ERT) and Vertical Electrical Sounding (VES) approves representative values for unconsolidated silts, muds and sand with a high degree of saline saturation from the periodic wet/dry cycles and annual flooding/desiccation. Figure 5.6 demonstrates a 3-D illustration of the ERT grid profiles at site 1 together with a location of core drilling bore hole 5(CB5) that was formerly taken at the area. The correspondence shown here, in particular between profile 6 and profile 1-5, provides a high level of assurance in the small changes noted in resistivity as replicating real changes in ground conditions. These changes possibly represent small dissimilarities in either the lithology and/or changes in ground water mineralization.

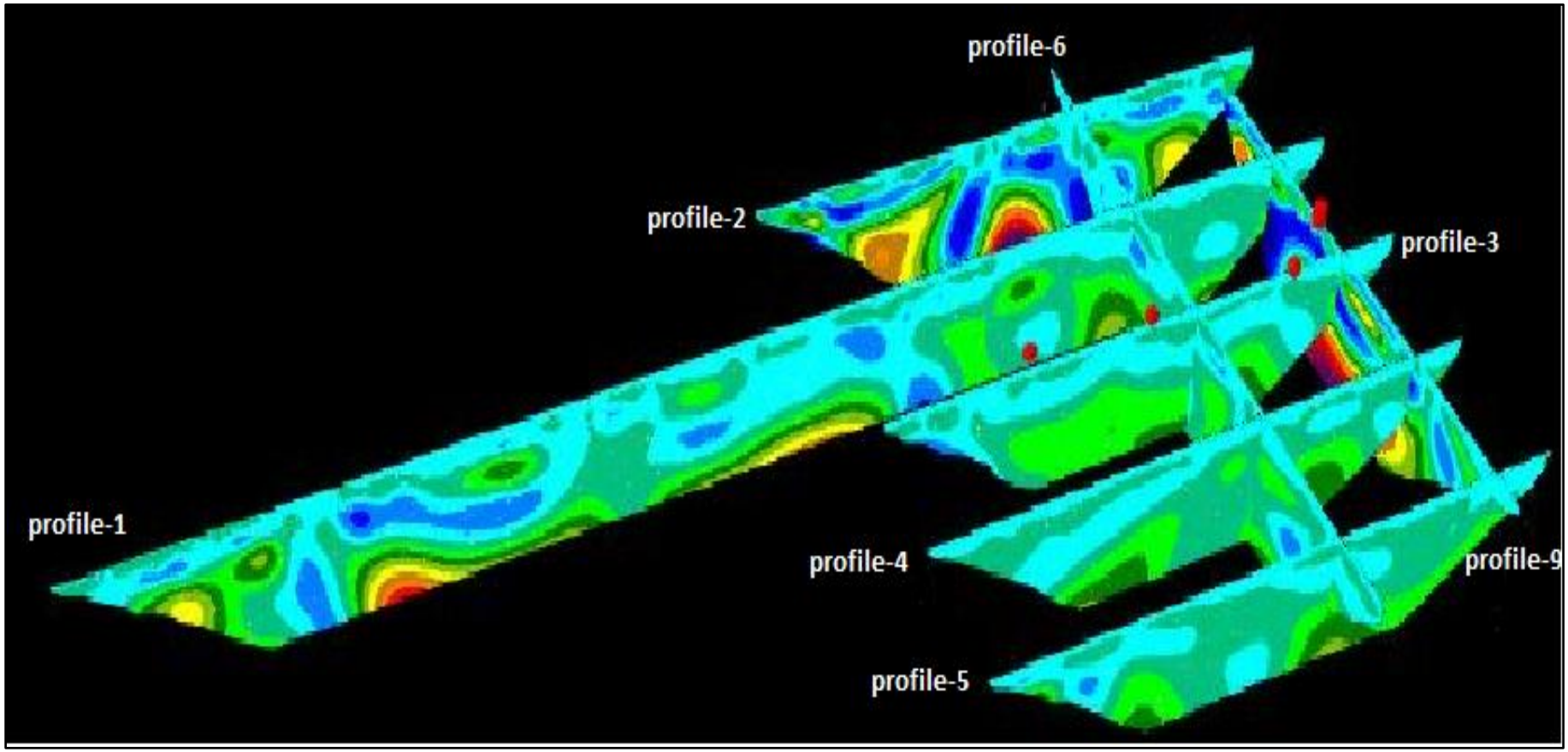

Figure 5. 6 ERT sections for Site 1. Red sphere are VES locations, red cylinder is CB5 core location.

At site-1 profile 2 and profile 9 indicates a higher variation in resistivity than distinguished along profiles 1, 3, 4, and 5 at the middle of the site. While CB5(core drilling borehole-5) does provide the possibility of some direct interpretation to the resistivity results, it is somewhat shallow depth (20 m) means that direct interpretation of each profile is rather hypothetical without further ground control. Correlation of CB5 (core drilling bore hole-5) with profile 9 for the first 20 m depth appears good and is shown in figure 5.6. Additional work on this interpretation is essential with the complete borehole results.

It is interesting to note the position of Site 1 with respect to the shallow depression that extends to the east as noted in the surface DTM. The presence of such large, shallow depressions or channels suggests that a drainage and desiccation history is not only manifest in the basin but that it could also be recorded within the deposits.

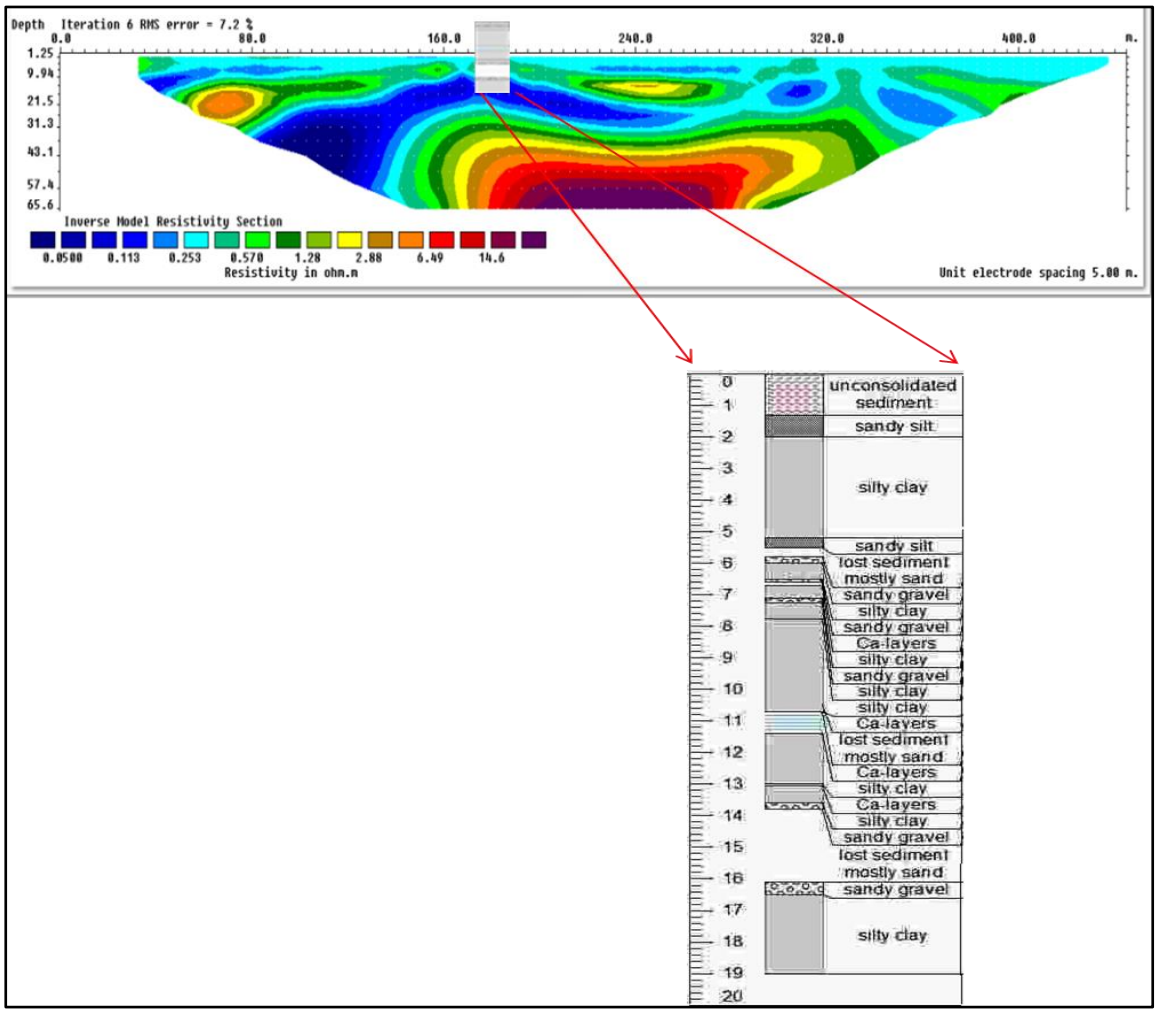

Figure 5. 7 Correlation of Line 9 and borehole data.

Site 2 confirms resistivity differences analogous to those perceived on profile 6 and 9 at site 1. The relationship at the intersection of the profiles is worthy (see figure 5.7), once more giving high assurance in the data.

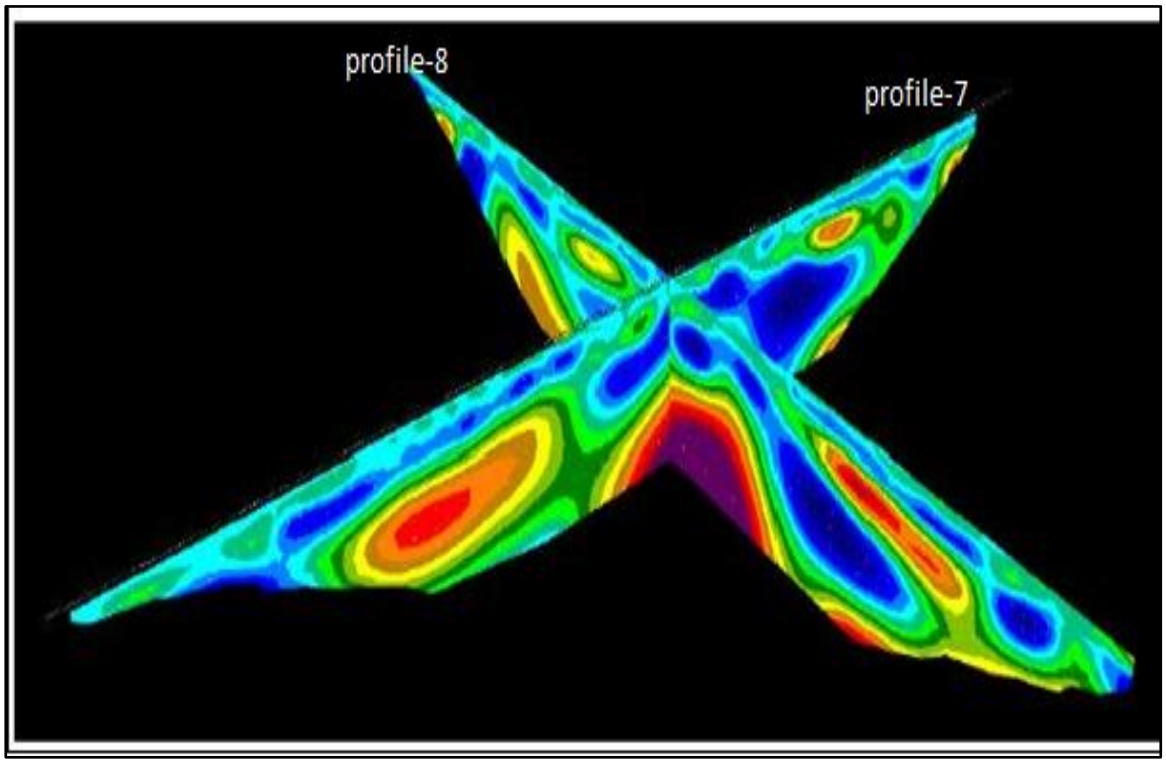

Figure 5. 8 ERT sections for Site 2.

Regardless of the small range of resistivity noted at Sites 1 and 2 the profile-ties across the grid provide confidence in the data such that the patterns appear to be marking real subsurface variations in geology. The shapes of the patterns or geometries are not those that would normally be associated with channel cuts: rather, the resistivity changes are interpreted as subtle changes within a dominantly layered sequence.

The main differences in resistivity were visible at site 3 along the profile from the alluvial material onto the basin floor. It was notable in the field that the alluvial fan comprised of fine to medium sand with large (up to 30 cm) clasts of both metamorphic and igneous material. This is consistent with the resistivity variations noted in the field which is greater than 500 ohm-m. Comparable resistivity results were not seen at either Site 1 or 2 and therefore it is suggested that, to the surveying depth verified here (to approximately 70-100m depth), the alluvial fans do not extend through the valley floor to these center basin locations.

CHAPTER SIX

6. CONCLUSIONS AND RECOMMENDATIONS

6.1 General

An integrated study involving basically electrical (VES and ERT) and seismic surveys were carried out at the chew Bahir dry Lake bed located in the southern extension of the east African rift valley in southern Ethiopia. The geophysical surveys: 2D electrical imaging and vertical electrical sounding were conducted and seismic data were taken from Tullow Oil Plc. for better assurance of the electrical surveys.

In the above Chapters of this thesis work, the survey profiles, the instruments employed techniques of data acquisition, interpretation of the results of those different techniques and their relevance to ongoing project and for the scientific community at large has been examined. In this chapter we present the summary of this work and give some concluding remarks about the work. A final section gives some recommendations for the drilling team of paleoenvironment reconstruction being currently undertaken and also adds some data sets of the area.

6.2 Conclusions

- Regional seismic acquired in the Chew Bahir basin indicates a sequence of unconsolidated, Lake Sediments extending to depths in excess of 5km at the basin center.
- The range of resistivity interpreted in both the ERT and VES shows representative values for unconsolidated silts, muds and sand with a high degree of saline saturation from the periodic wet/dry cycles and annual flooding/desiccation.
- The largest variations in resistivity were marked at site 3 along the traverse from the alluvial material onto the basin floor. It was noted in the field that the alluvial fan consisted of fine to medium sand with large (up to 30 cm) clasts of both metamorphic and igneous material. This is consistent with the resistivity variations noted in the field which is greater than 500 ohm-m.
- Due to the very conductivity of the sub surface of the study area, the depth anticipated for vertical electrical sounding (VES) survey couldn't be achieved.
- Electrical resistivity results suggest fine-grained deposits with high evaporite content.

- Small variability in resistivity is interpreted as either desiccation inhomogeneity or variability in lithology as a result of flooding/desiccation history.
- No indication of alluvial fan deposits were recorded at the basin center sites.

6.3 Recommendations

- High resolution seismic reflection survey to be undertaken before drilling at the site will aim to address the ambiguity of being desiccation inhomogeneity or variability in lithology.
- On the basis of seeking a location for drilling that is relatively free of lateral inhomogeneity and comprises a conformable resistivity 'stratigraphy', Site 1 at UTM (261829, 521120) is recommended for the main drilling site.
- Correlation of CB5(core drilling borehole) with profile 9 for the first 20m depth appears good and is shown in figure 5.6 further works on this interpretation is required with the full borehole results.

References

1. **Camberlin, P., (1997)**. Rainfall anomalies in the source region of the Nile and their connection with the Indian summer monsoon. Journal of Climate **10**, 1380-1392.
2. **Camberlin, P., Philippon, N., (2002).** The East African March-May rainy season: associated atmospheric dynamics and predictability over the 1968-97 periods. Journal of Climate **15**:1002-1019.
3. **Chorowicz, J.,Collet, B., Bonavia,.F.,and Tesfaye Korme, (1994).** Northwest to north-northwest extension direction in the Ethiopian Rift deduced from the orientation of extension structures and fault-slip analysis. Geological Society of America Bulletin. **105**:1560–1570.
4. **Davidson, A., (1983).** The Omo River Project: reconnaissance geology and geochemistry of parts of Ilubabor. Kefa, Gemu Gofa, and Sidamo. Ethiopian Institute of Geological Survey Bulletin.**2**:1-89.
5. **Davidson, A.,and Rex, D.C., (1980).** Age of volcanism and rifting in southwestern Ethiopia. Nature. **283**:657–658.
6. **Dobrin, M.B. and Savit, C. H., (1988).** Introduction to geophysical prospecting, fourth edition. McGraw-Hill, New York, USA .PP498-613,750-837.
7. **Ebinger, C.J., Harding, D., Samson Tesfaye., Kelley, S., Rex, D., (2000).** Rift deflection, migration, and propagation: linkage of the Ethiopian and Eastern rifts, Africa. Geological Society of America Bulletin **112**, 163-176.
8. **Foester, V, Junginger, A., Langkamp, O., Tsige Gebru, , Asfawossen Asrat, Mohammed Umer, M., Lamb, H.,Wennrick, V., Rethemeyer, J., Nowaczyk, N., Trauth, M. and Schaebitz, F.,(2012).** Climate change recorded in the sediments of the Chew Bahir bain, southern Ethiopia, during the last 45,000 years. Quaternary International **274**:25-37.
9. **Geotomo Software (2006).** RES2DINV Ver. 3.55, Rapid 2-D Resistivity and IP inversion using the least-squares method (available at www.geoelectrical.com).
10. **Gibson I., (1969).** The structure and volcanic geology of an axial portion of the Main Ethiopian Rift, Tectonophysics. **8**:561–565.
11. **Gibson, P.J. and George, D.M., (2003).** Environmental applications of geophysical surveying techniques. Nova Science Publishers, Inc. New York.

12. **Gidey Woldegabriel, White, T., and Suwa, G., (1991).** Age of volcanism and fossils in the Burji–Soyoma area, Amaro Horst, southern Main Ethiopian Rift. J. Afr. Earth Sci. **13**: 437–447.
13. **Golden software, (2010).** User manual of Surfer, version 9.11.
14. **Griffiths, D.H. and Barker, R.D., (1993).** Two-dimensional resistivity imaging and modeling in areas of complex geology. Journal of Applied Geophysics, **29**: 211-226.
15. **Keller, G.V. and Frischknecht, F.C., (1966).** Electrical Methods in Geophysical Prospecting. Pergamon Press, Oxford, pp501-519.
16. **Knapp RW, Steeples D.W., (1986b):** High-resolution common-depth-point reflection profiling–Field acquisition parameter design. –Geophysics **51**: 283–294.
17. **Kunetz, G., (1996).** Principles of direct current resistivity prospecting. Gebruder-Borntrager, Berlin- Nikolassee, pp103.
18. **Loke, M. H. and Dahlin, T., (2002).** A comparison of the Gauss-Newton and quasi-Newton methods in resistivity imaging inversion. Journal of Applied Geophysics, **49**: 149-162.
19. **Loke, M.H., (1997).** Electrical imaging surveys for environmental and engineering studies: a practical guide to 2D and 3D surveys: Unpublished short training course lecture notes, University of Sains Malaysia, Penang, Malaysia pp1-50.
20. **Loke, M.H., (1999).** Electrical imaging surveys for environmental and engineering studies. A practical guide to 2-D and 3-D surveys, Penang, Malaysia, pp1-57.
21. **Lowrie, W., (2007).** Fundamentals of Geophysics Second Edition Cambridge, New York, pp282 – 360
22. **McSweeney, C., New, M. and Lizcano, G., (2010).** UNDP Climate Change Country Profiles, Ethiopia. http://country-pr=ofiles.geog.ox.ac.uk/ accessed on 24.6.2013.
23. **Mohr, P.A., (1970).** The Geology of Ethiopia. Addis Ababa University Press, Addis Ababa. pp. l-268.
24. **Mohr, P.A., (1987).**Patterns of faulting in the Ethiopian rift valley. Tectonophysics.**143**:169-179.
25. **Nicholson, S.E., (1996).** A review of climate dynamics and climate variability in Eastern Africa. In: Johnson, T.C., Odada, E.O. (Eds.), The Limnology, Climatology and Paleoclimatology of the East African Lakes. Gordon & Breach, Amsterdam, pp. 25-56.
26. **Reynolds, J.M., (1997).** An Introduction to Applied and Environmental Geophysics. John Wiley and Sons limited, England, UK. pp. 116-209, 415-522.

27. **Sasaki, Y., (1992).** Resolution of resistivity tomography inferred from numerical simulation. Geophysical Prospecting, **40**: 453–46.
28. **Segele, Z.T., Lamb, P.J., (2005)**. Characterization and variability of Kiremt rainy season over Ethiopia. Meteorology and Atmospheric Physics **89**, 153-180.
29. **Sheriff, R.E., (2002).** Encyclopedic Dictionary of Exploration Geophysics (4th ed.). – Soc. Of Expl. Geophys. Tulsa, USA.
30. **Steeples, D.W. and Miller R.D., (1998).** Avoiding pitfalls in shallow seismic reflection surveys. Geophysics **63**: 1213–1224.
31. **Telford, W.M., Geldart, L.P. and Sheriff, R.E., (1990).** Applied Geophysics, 2nd Edition; Cambridge University Press, Cambridge, UK. pp. 6-48,522-562.
32. **Tigistu Haile, (2010).** Applications of Electrical Resistivity Tomography (at www.mawari.net).
33. **Wolke, R. and Schwetlick, H., (1988).** Iteratively reweighted least squares algorithms, convergence analysis, and numerical comparisons. SIAM Journal of Scientific and Statistical Computations. **9**: 907-921.
34. **Yilmaz, O., (2001).** Seismic Data Analysis (**1** and **2**; 2nd ed.). – Soc. of Expl. Geophys. Tulsa, USA.

APPENDICIES

Appendix 1 Geographical coordinates of Earth Resistivity tomography (ERT) data points

P. No		**Electrode No.**												
P-1		1	18/19	36/37	54/55	72	90	108	126	144	162	180	198	216
	Easting	262132	261957	262046	261865	261776	261687	261598	261418	261327	261239	261151	260967	260970
	Northing	521398	521422	521408	521432	521445	521459	521471	521494	521509	521521	261060	521545	521555
	Elevation	501	501	501	500	501	501	500	501	502	501	500	500	501
P-2	Easting	262117	262029	261940	261851	261761	261671	261581						
	Northing	521495	521507	521522	521534	521547	521558	261581						
	Elevation	500	500	500	500	501	500	500						
p-3	Easting	262053	261967	261878	261788	261701	261612	261524						
	Northing	521091	521103	521116	521127	521138	521154	521162						
	Elevation	500	500	500	500	500	500	500						
p-4	Easting	262154	262067	261979	261891	261800	261711	261625						
	Northing	521203	521213	521224	521236	521248	521258	521272						
	Elevation	501	501	501	501	501	500	500						
p-5	Easting	262171	262082	261994	261904	261814	261725	261636						

	Northing	521101	521112	521124	521136	521149	521162	521174						
	Elevation	501	501	501	501	501	501	501						
p-6	Easting	261956	261946	261936	261925	261915	261904	261894						
	Northing	521046	521132	521220	521310	521400	521489	521577						
	Elevation	500	501	500	501	501	500	501						
p-7	Easting	258649	258649	258648	258649	258650	258649	258649						
	Northing	521861	521949	522039	522130	522218	522310	522398						
	Elevation	500	500	500	500	500	500	500						
p-8	Easting	258915	258827	258739	258648	258557	258467	258379						
	Northing	522133	522132	522130	522130	522129	522128	522127						
	Elevation	500	500	500	500	500	500	500						
p-9	Easting	262041	262052	262061	262073	262082	262093							
	Northing	521520	521433	521343	521254	521165	521076							
	Elevation	501	501	501	501	500	500							

Appendix 2 Vertical Electrical sounding (VES) raw data

					Apparent Resistivity in ohm-m for AB/2																
No	VES index	UTM East	UTM north	Elv.	1.5	2.1	3	4.2	6	9	13.5	20	30	45	66	100	150	220	330	500	750	1000
1	Chb-1	262053	521091	501	5	0.5	0.3	0.2	0.3	0.3	0.3	0.02	0.4	0.4	0.4	0.2	0.6	0.7	0.9	1.3	2.5	5.1
2	Chb-2	261878	521116	501	0.5	0.4	0.3	0.3	0.3	0.3	0.3	0.4	0.4	0.5	0.6	0.6	0.6	0.8	1.2	1.9	2.78	1.66
3	Chb-3	261701	521138	501	0.5	0.5	0.4	0.4	0.4	0.3	0.3	0.4	0.4	0.6	0.7	0.2	0.5	0.4	1.0	0.8	2.18	3.77

Appendix 3 Resistivity of some common rocks, minerals and soils (Loke, 2004)

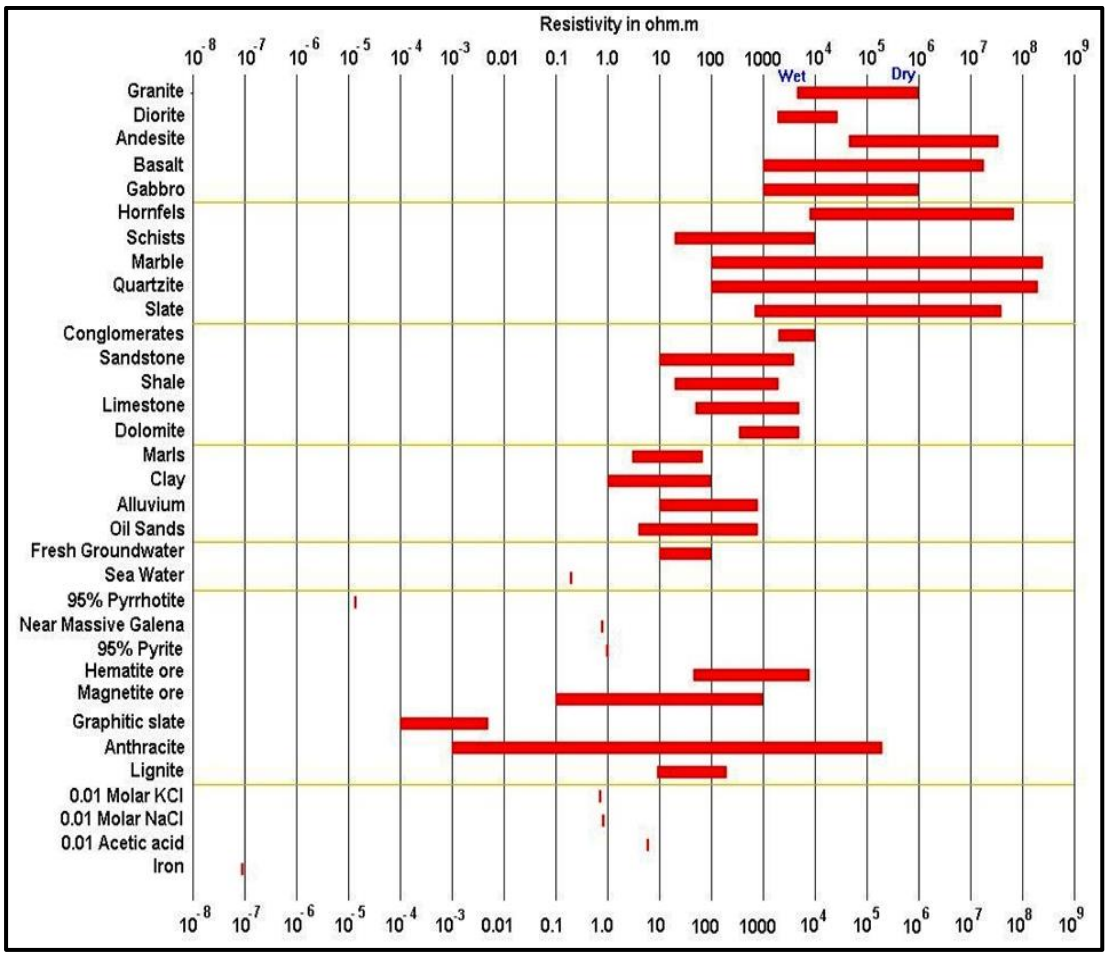

Appendix 4 Measured, calculated and inverted electrical sections

Profile 1

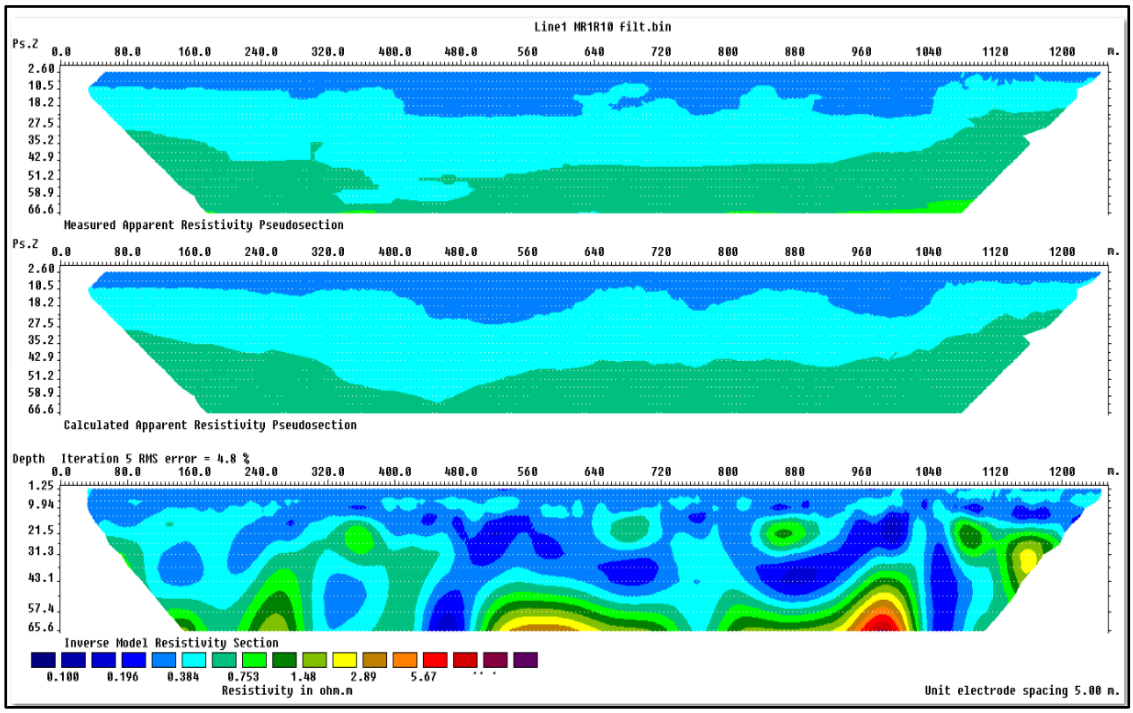

Profile 2

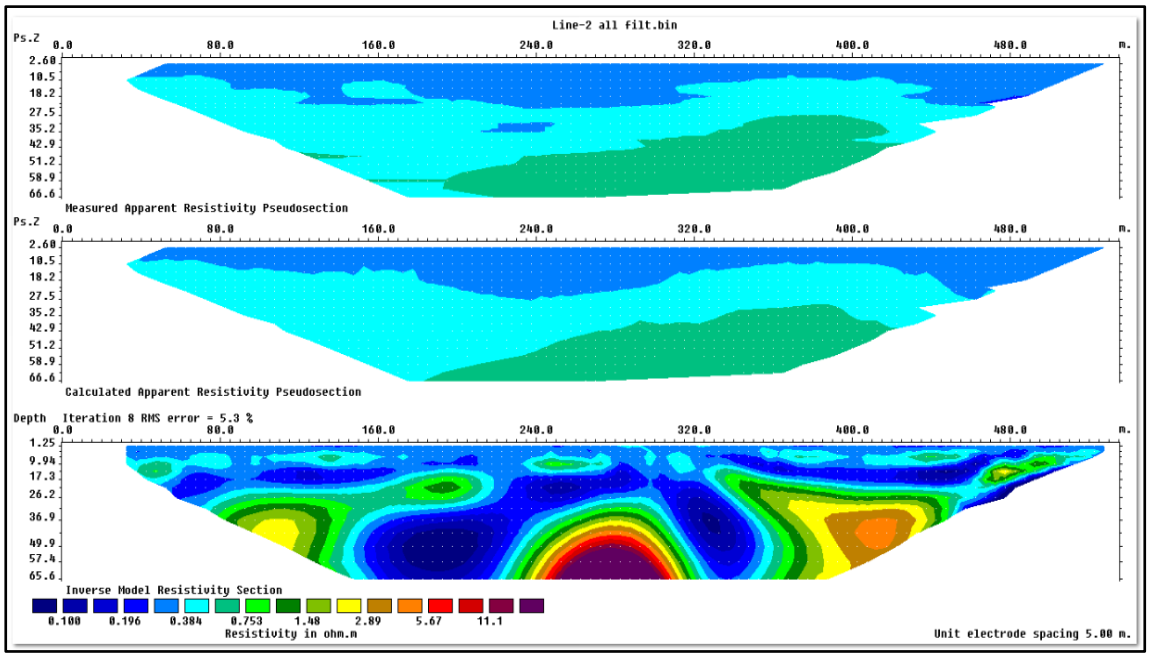

Profile 3

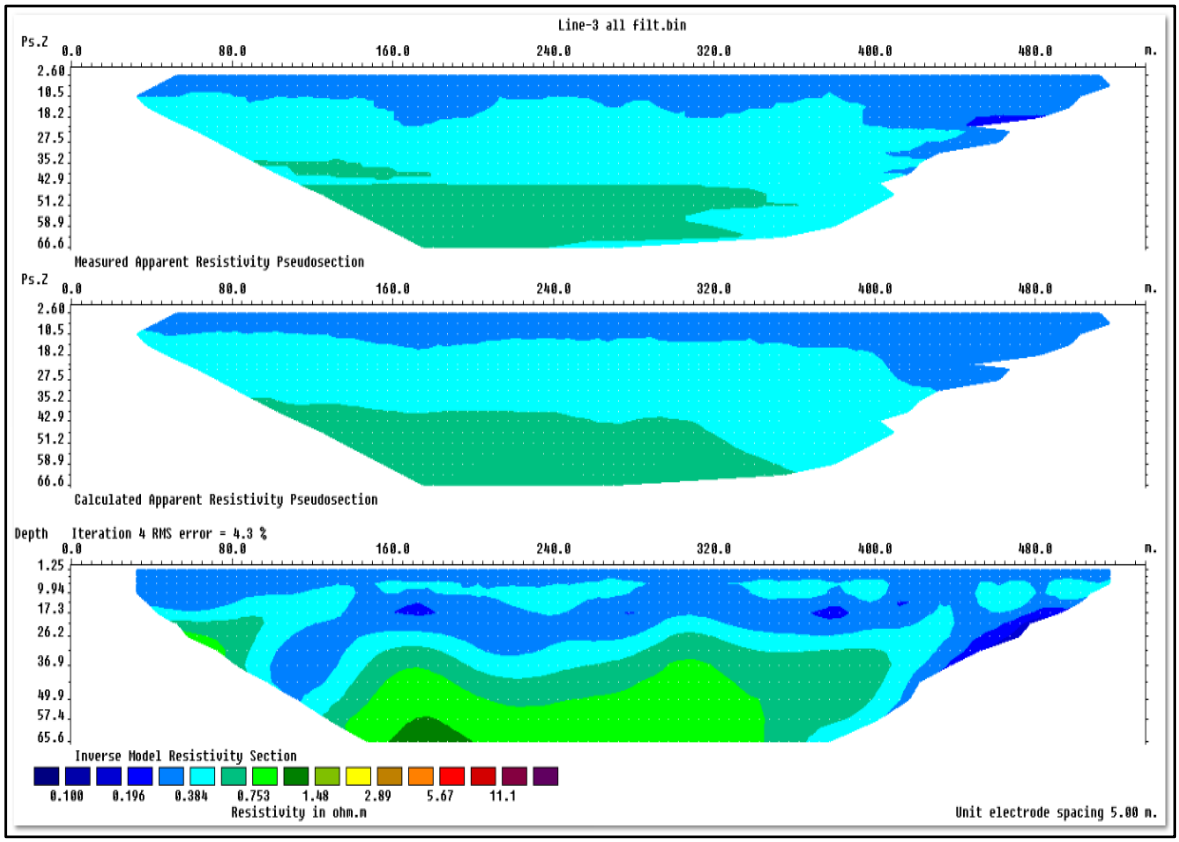

Profile 4

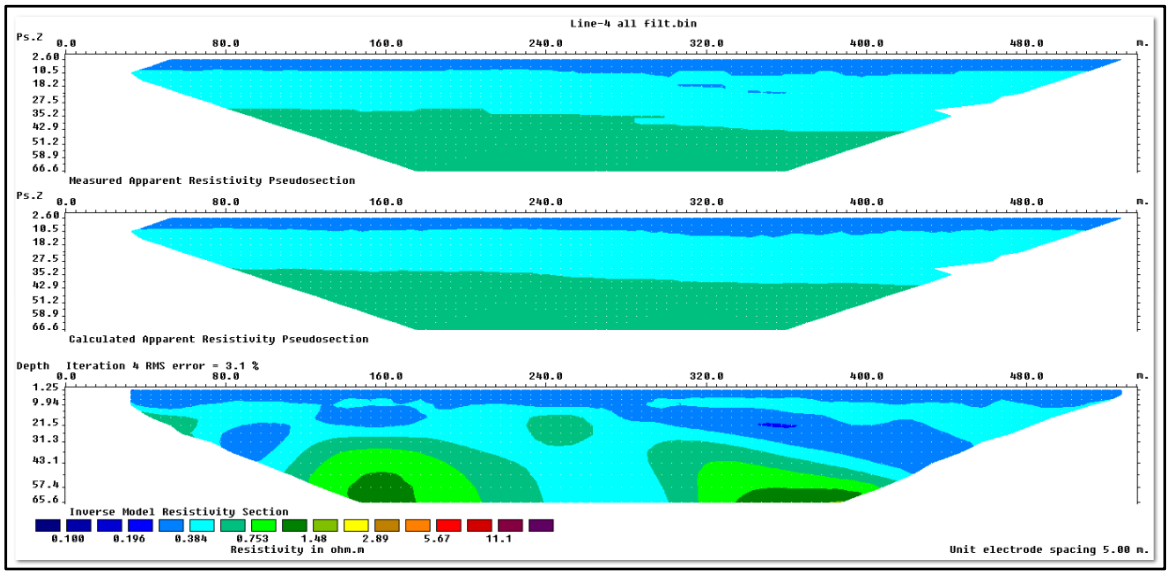

Profile 5

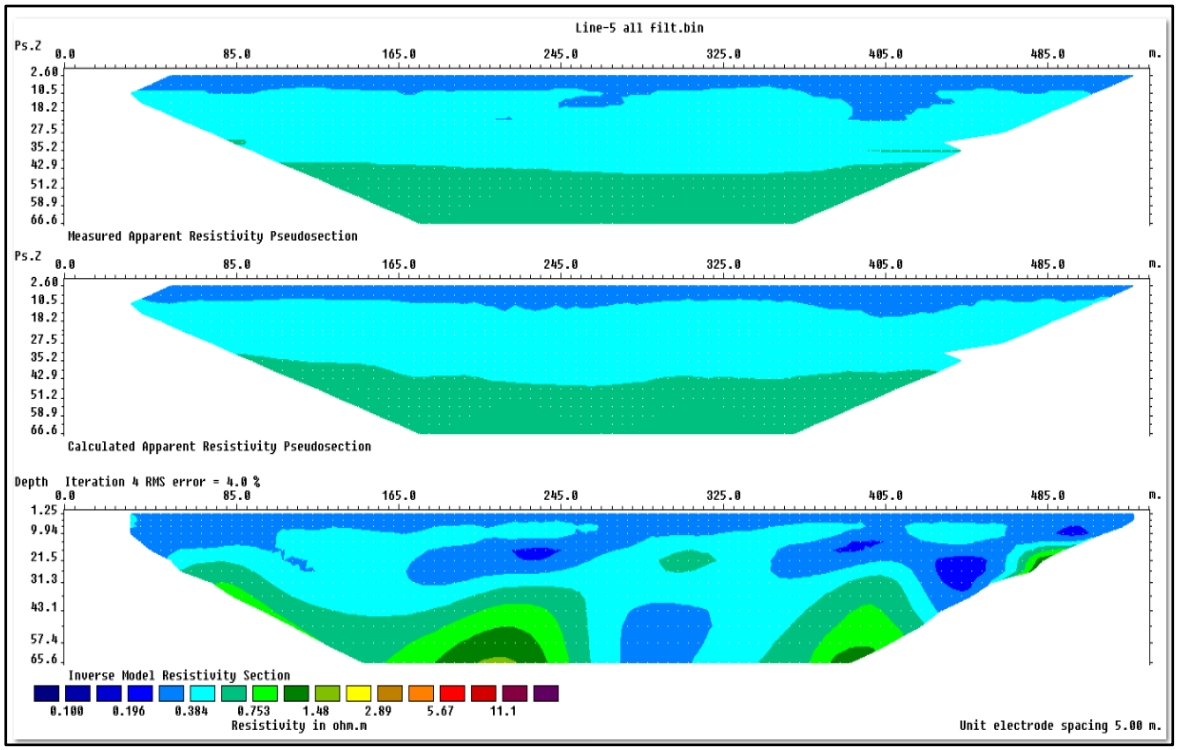

Profile 6

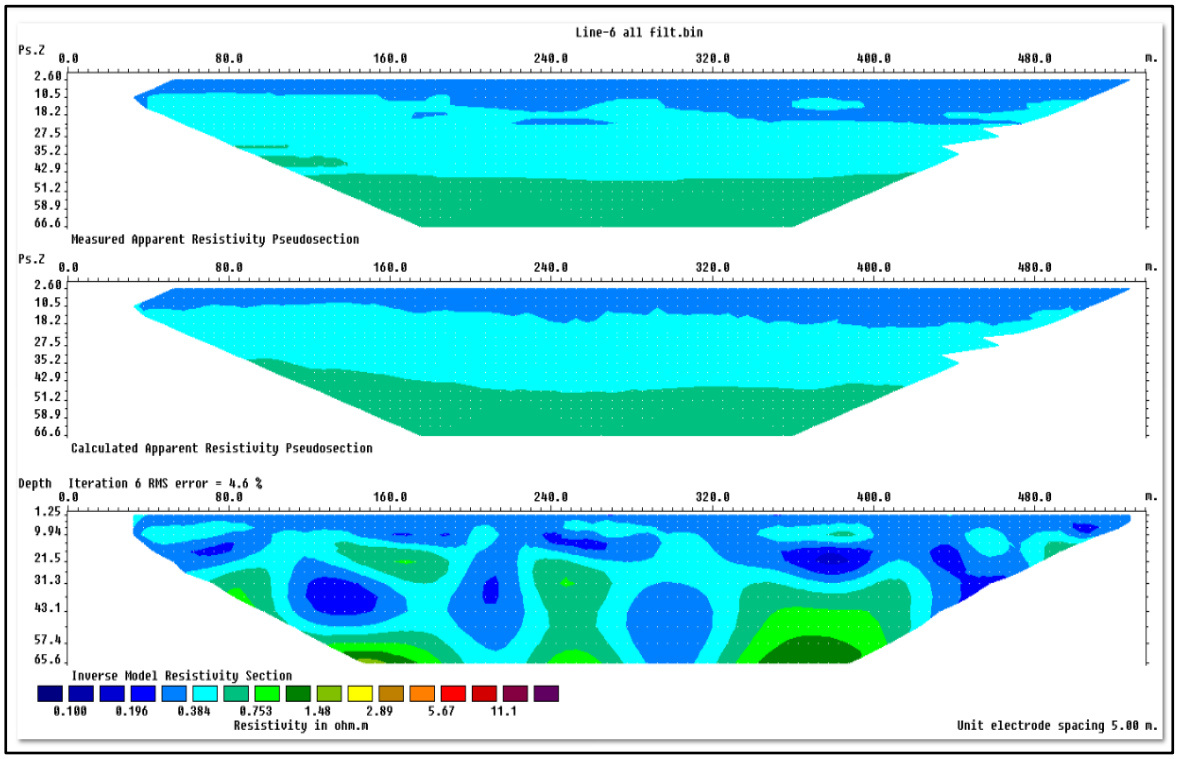

Profile 7

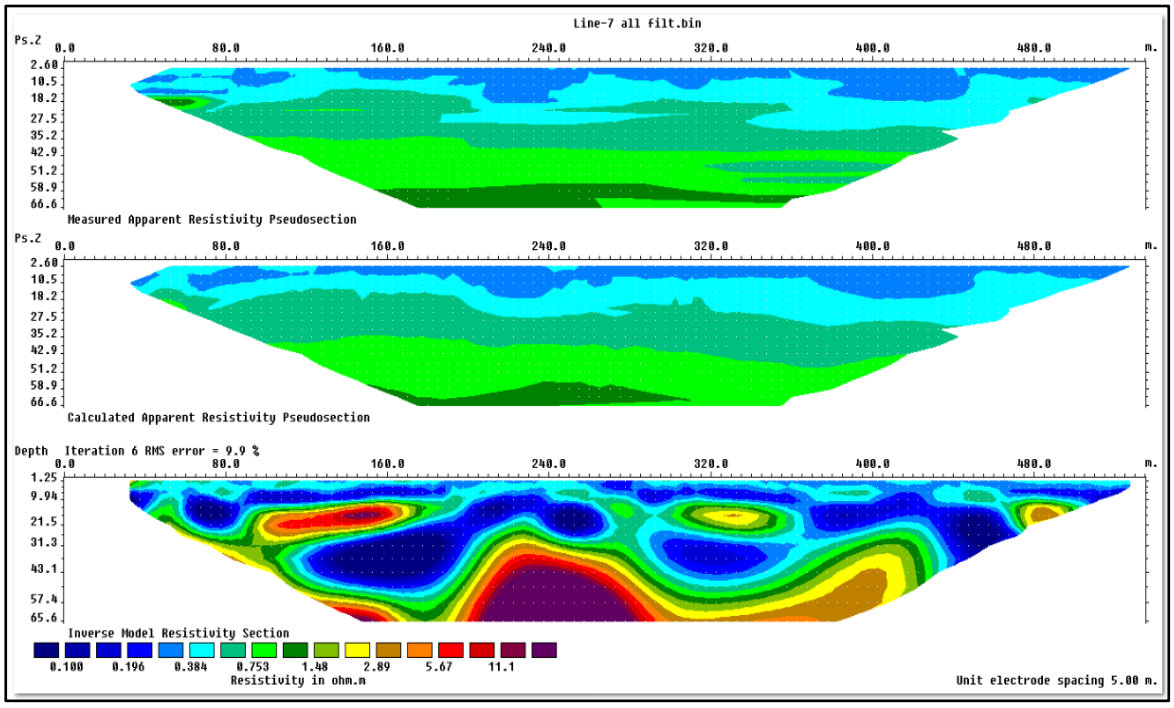

Profile 8

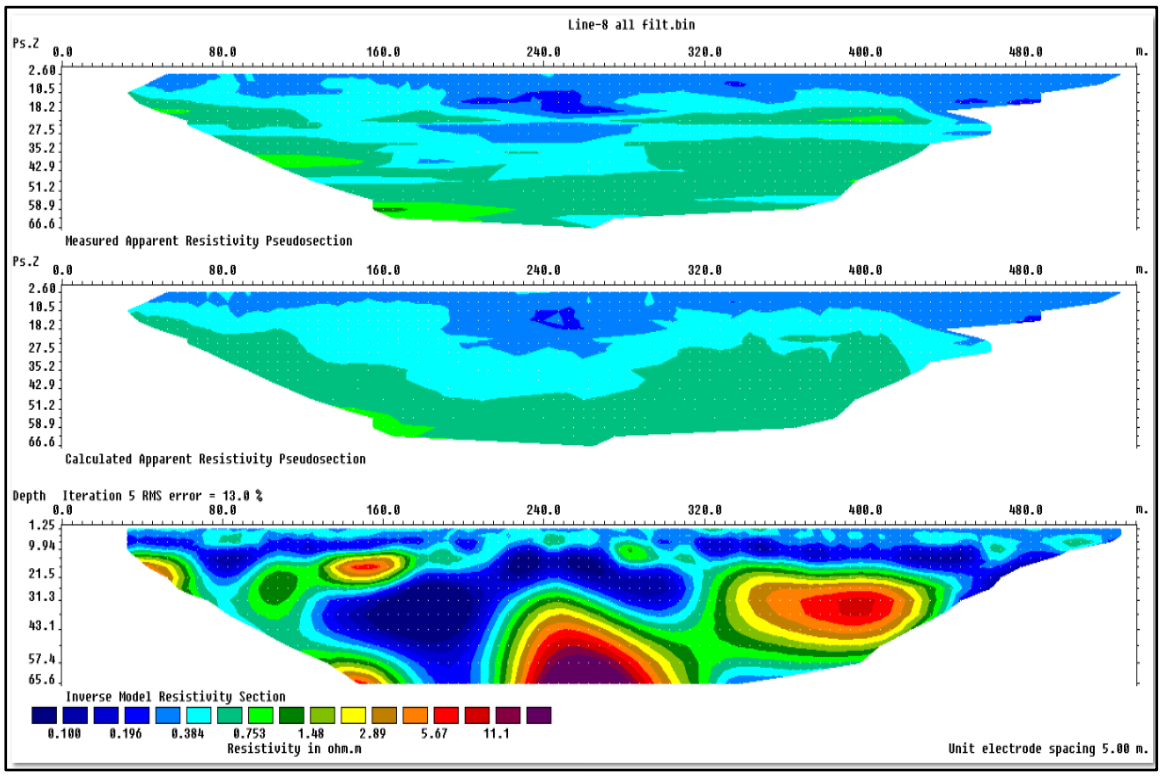

Profile 9

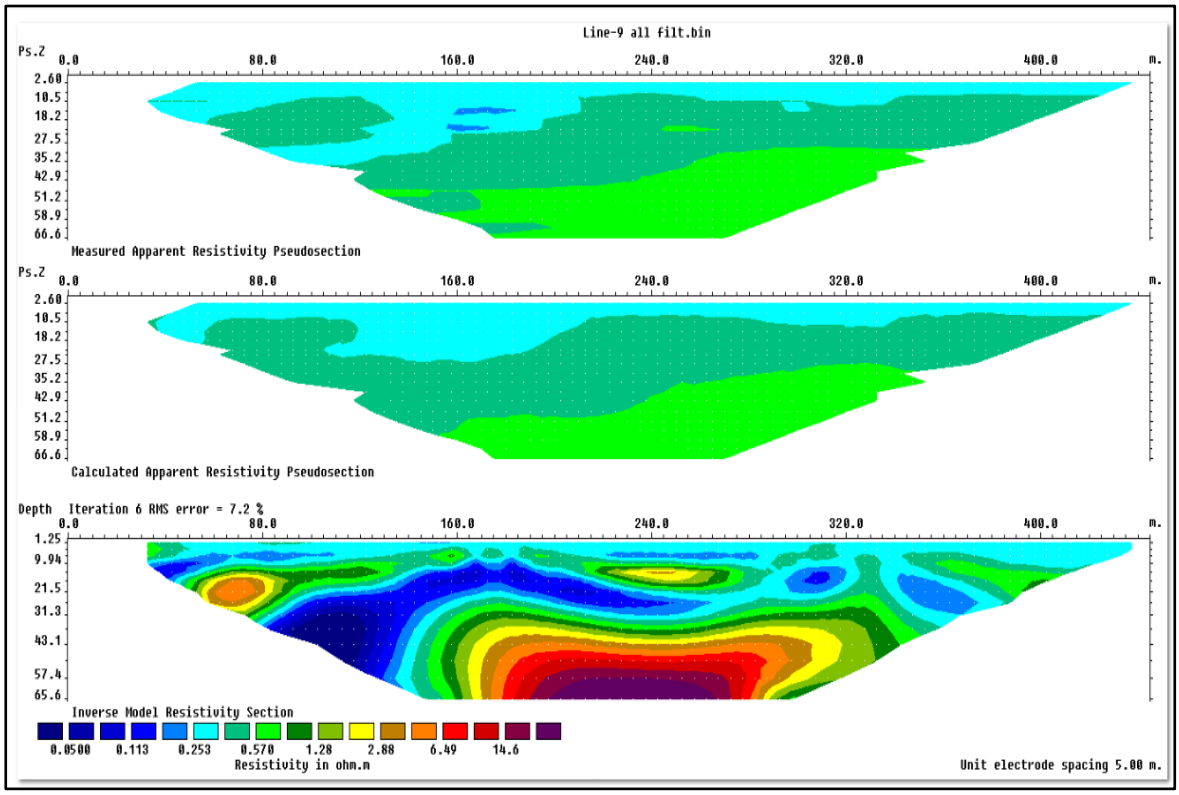

Profile 10

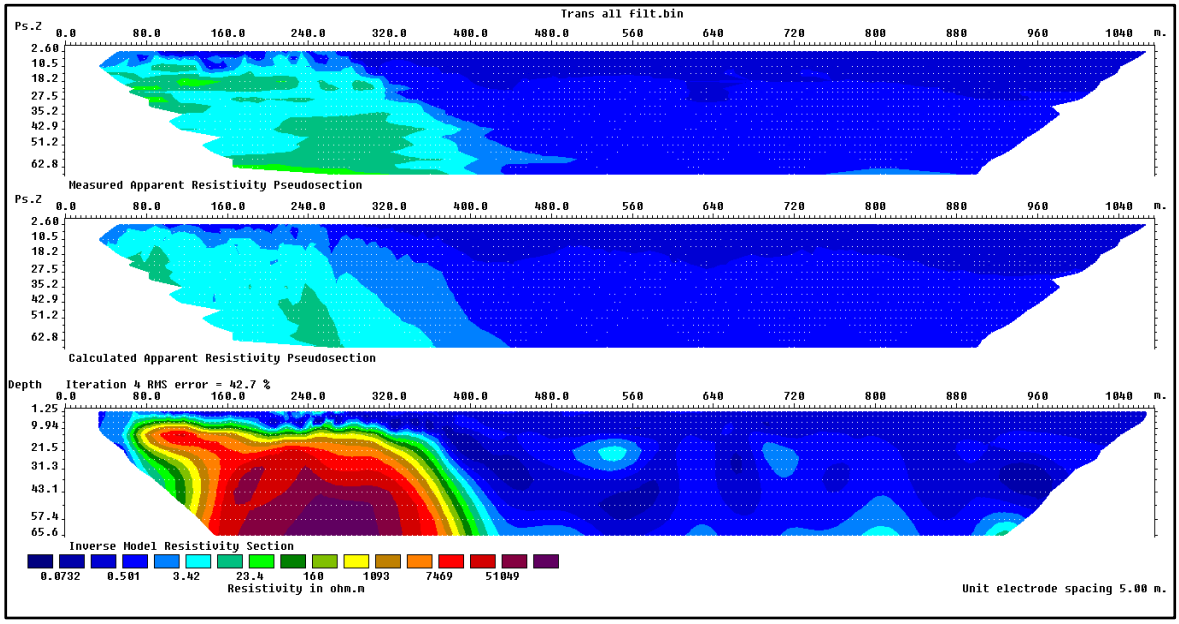

Appendix 5 Tullow oil seismic line acquisition

Tullow Ethiopia 2D Seismic Progress Map

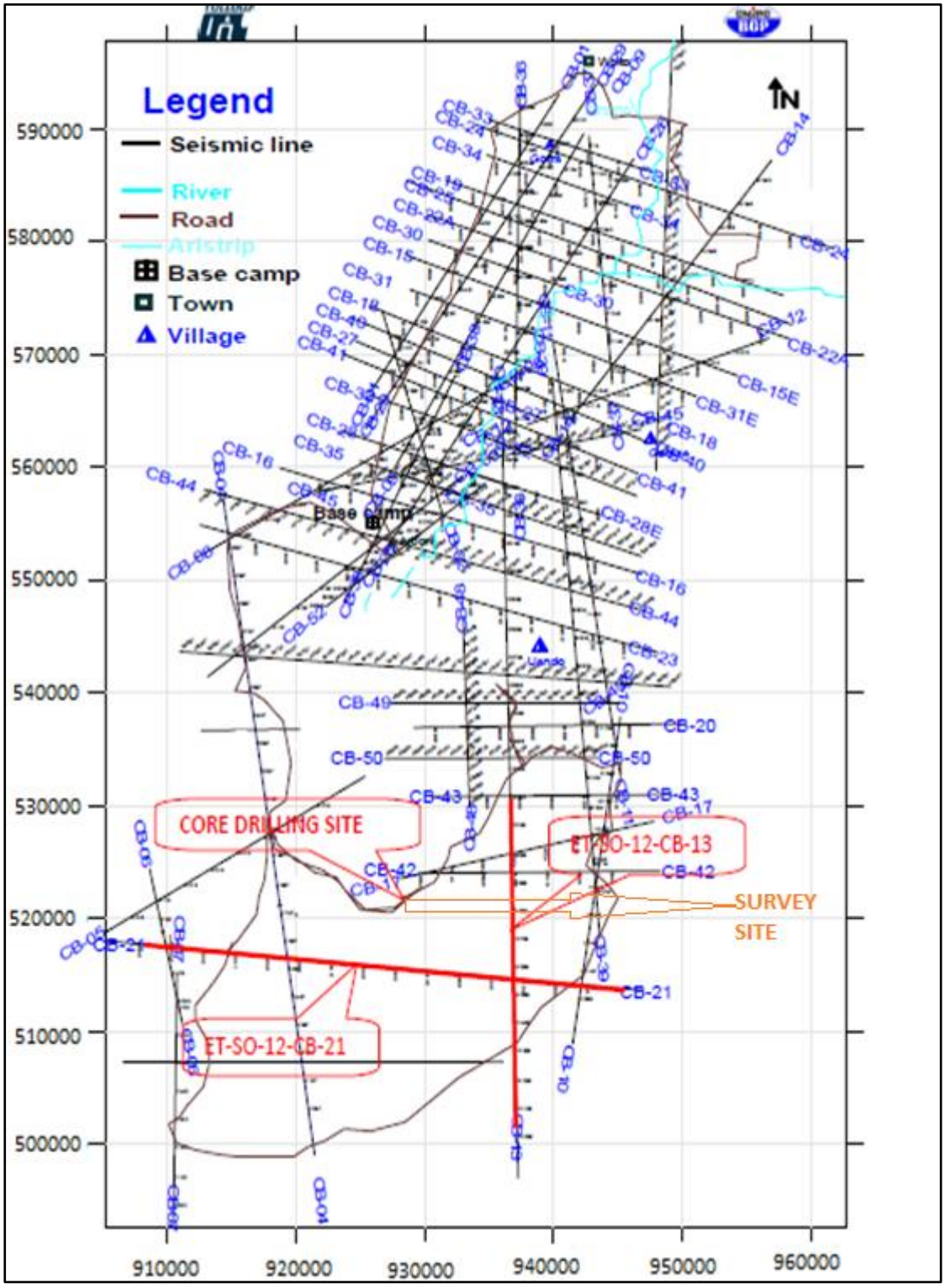

Appendix 6 Tullow oil seismic reflection Profile 21

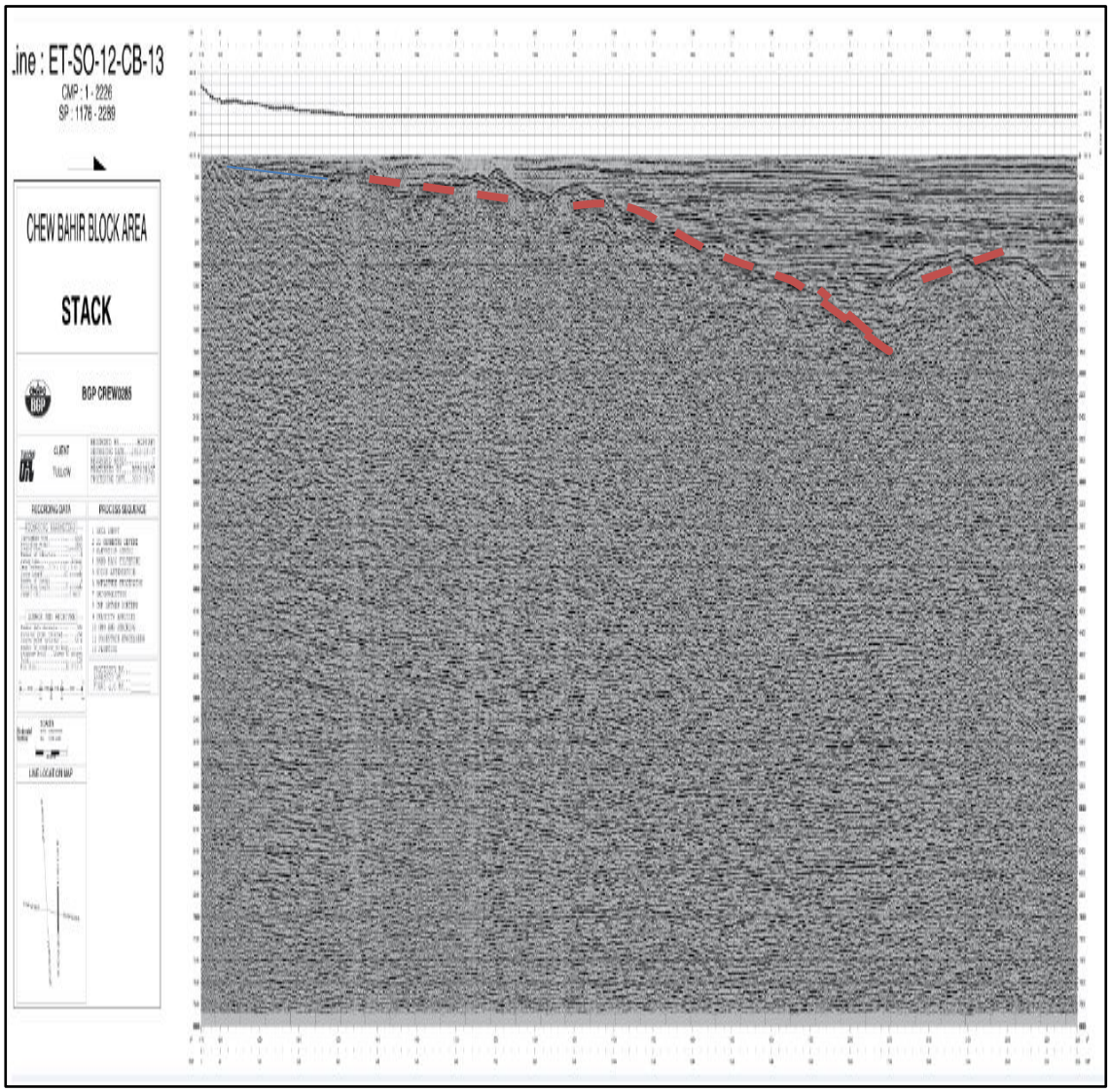

Appendix 7 Tullow oil seismic reflection Profile 13

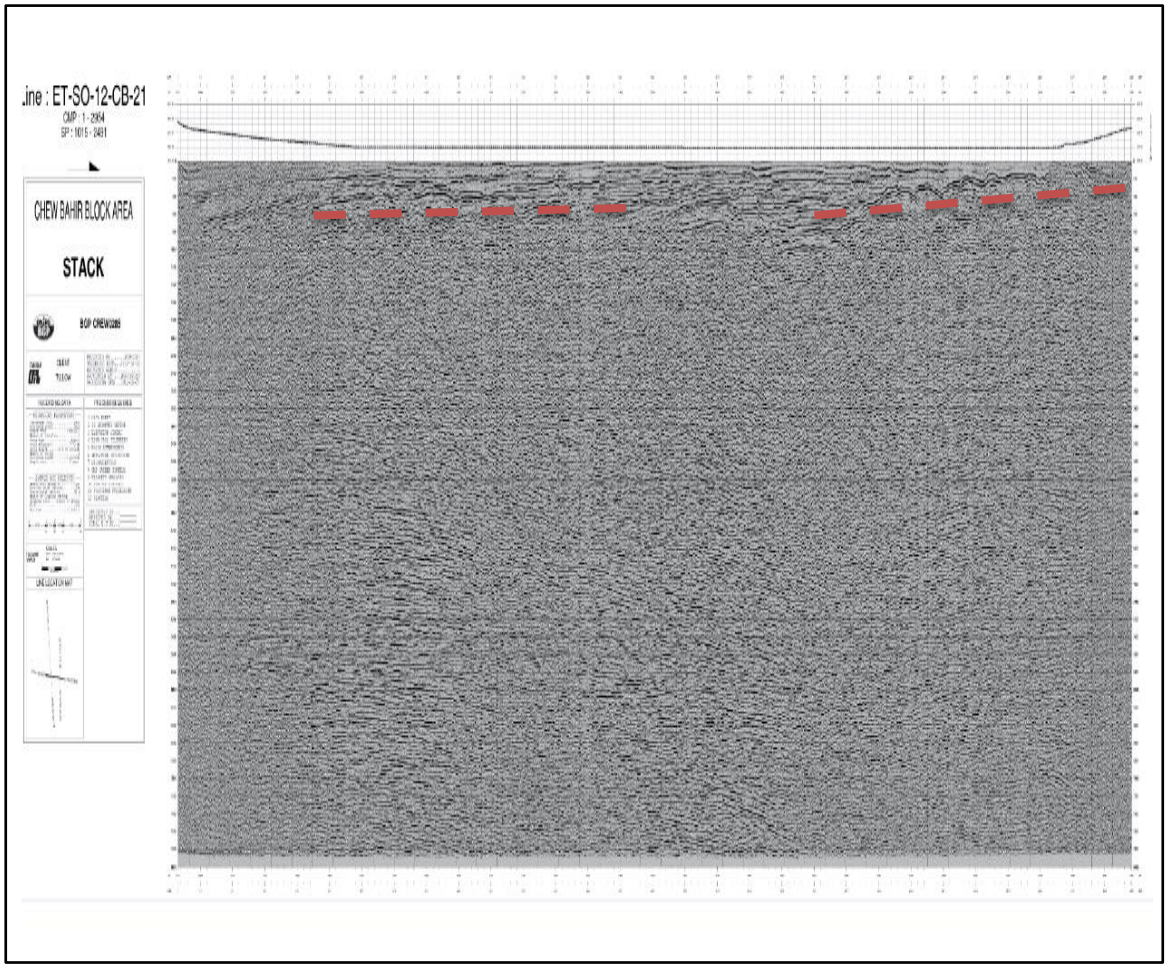

Appendix 8 Lithological description of bore hole

Lithological description of CB-5

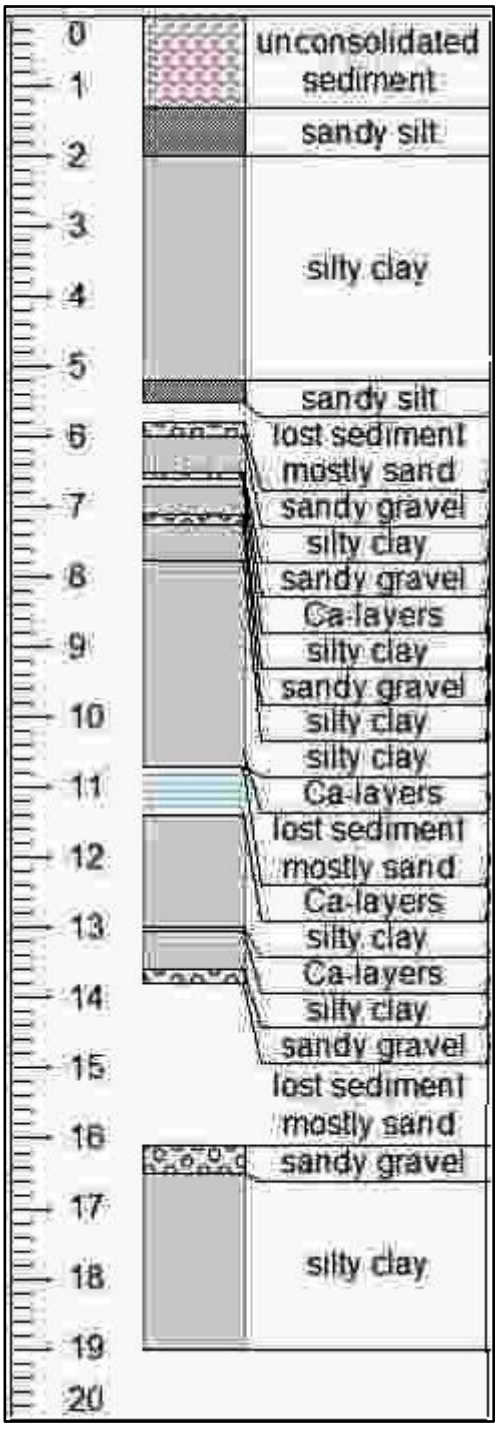

Declaration

I hereby declare that the thesis entitled "Integrated Geophysical Investigation for Chew Bahir Lake Bed Characterization, Southern Ethiopia" has been carried out by me under the supervision of Dr. Tigistu Haile during the year 2013/14 as part of Master of Science program in Exploration Geophysics. I further declare that this work has not been submitted to any other University or institution for the award of any degree or diploma and all sources of material used for the thesis have been duly acknowledged.

Daniel Mamo Teshome

Signature _____

Place and date of submission: School of Earth Sciences, Addis Ababa University

December, 2014